



## Article

# A New Nanomaterial Based Biosensor for MUC1 Biomarker Detection in Early Diagnosis, Tumor Progression and Treatment of Cancer

Fulden Ulucan-Karnak <sup>1,2,\*</sup> and Sinan Akgöl <sup>2</sup>

<sup>1</sup> Biomedical Technology Department, Graduate School of Applied and Natural Sciences, Ege University, Izmir 35040, Turkey

<sup>2</sup> Department of Biochemistry, Faculty of Science, Ege University, Izmir 35040, Turkey; sinan.akgol@ege.edu.tr

\* Correspondence: ulucanfulden@gmail.com

**Abstract:** Early detection of cancer disease is vital to the successful treatment, follow-up and survival of patients, therefore sensitive and specific methods are still required. Mucin 1 (MUC1) is a clinically approved biomarker for determining the cancer that is a type I transmembrane protein with a dense glycosylated extracellular domain extending from the cell surface to 200–500 nm. In this study, nanopolymers were designed with a lectin affinity-based recognition system for MUC1 detection as a bioactive layer on electrochemical biosensor electrode surfaces. They were synthesized using a mini emulsion polymerization method and derivatized with triethoxy-3-(2-imidazolin-1-yl) propylsilane (IMEO) and functionalized with Concanavalin a Type IV (Con A) lectin. Advanced characterization studies of nanopolymers were performed. The operating conditions of the sensor system have been optimized. Biosensor validation studies were performed. Real sample blood serum was analyzed and this new method compared with a commercially available medical diagnostic kit (Enzyme-Linked ImmunoSorbent Assay-ELISA). The new generation nanopolymeric material has been shown to be an affordable, sensitive, reliable and rapid device with 0.1–100 U/mL linear range and 20 min response time.

**Keywords:** MUC1; cancer biosensor; polymeric nanomaterials



**Citation:** Ulucan-Karnak, F.; Akgöl, S. A New Nanomaterial Based Biosensor for MUC1 Biomarker Detection in Early Diagnosis, Tumor Progression and Treatment of Cancer. *Nanomanufacturing* **2021**, *1*, 14–38. <https://doi.org/10.3390/nanomanufacturing1010003>

Academic Editor:  
Andres Castellanos-Gomez

Received: 14 March 2021  
Accepted: 27 April 2021  
Published: 13 May 2021

**Publisher's Note:** MDPI stays neutral with regard to jurisdictional claims in published maps and institutional affiliations.



**Copyright:** © 2021 by the authors. Licensee MDPI, Basel, Switzerland. This article is an open access article distributed under the terms and conditions of the Creative Commons Attribution (CC BY) license (<https://creativecommons.org/licenses/by/4.0/>).

## 1. Introduction

Cancer is known as a complex disease with a large number of temporospatial changes in cell physiology, ultimately leading to malignant tumors [1]. Prostate, lung and colorectal cancers (CRCs) clarify for 43% (prostate 21%, lung 13%, colorectal 9%) of all cases in men in 2020 and 46% (prostate 26%, lung 12%, colorectal 8%) in 2021, with only prostate cancer having more than 1 in 5 new diagnoses. The three most common cancers for women are breast, lung and colorectal cancers. Most death is caused by lung, prostate and colorectum in men and lung, breast and colorectal cancer in women. Almost a quarter of all cancer deaths are caused by lung cancer [2–4].

Cancer is traditionally diagnosed by several imaging technologies, biopsy and detection of biomarkers. Using of imaging technologies such as X-ray, ultrasonography, computer tomography requires large tumors. In most cases, they can be imaged when the tumor reaches a diameter of 1 cm or a weight of about 1 g. Since these methods require long processes, early diagnosis of the disease is not very possible [5]. Magnetic resonance imaging (MRI) can produce three-dimensional, multimodal images without any use of ionizing radiation, providing an unprecedented accuracy in tumor examination. In addition, structural and functional MRI provides a more comprehensive assessment of the spread and activity of neoplastic diseases. A remarkable oncological condition assessment allows the creation of better therapeutic strategies with a positive effect on prognosis and survival [6,7]. Positron Emission Tomography/Computer Tomography (PET/CT) fusion

images provide higher diagnostic accuracy with less uncertain findings. This causes a greater impact on cancer diagnosis [8]. However, histopathological studies are required to confirm the results of PET-CT and MRI examinations [9].

Early diagnosis of cancer is vital for the successful follow-up of the disease and survival of patients, so precise and specific methods are required for early diagnosis. Analysis of biomarkers in blood, urine and other body fluids is one of the methods used in determining the disease [10]. An ideal biomarker should meet different criteria, such as: high sensitivity and specificity (detectable only in a single tumor type), levels associated with disease severity (surrounded by predictive and prognostic values) that cannot be detected in physiological processes or benign pathological conditions [11]. MUC1, the biomarker we used, was also approved in 1997 from Food and Drug Administration (FDA) and used in routine tests [12].

Mucin family are high molecular weight glycoproteins expressed by apical cell surface of epithelia. In contrast of healthy cells, tumor cells show significant loss of cell polarization and overexpression [13]. The human mucin (MUC) family have several members MUC1 to MUC21 and they have been sub-classified as secreted and transmembrane forms. The secreted mucins (for example, MUC2, MUC5AC, MUC5B and MUC6) form a physical barrier for organs such as the liver, breast, pancreas and kidney. The transmembrane mucins (for example, MUC1, MUC4, MUC13 and MUC16) have a single membrane-spanning region and related to the protective mucous gel via O-glycosylated tandem repeats that form rod-like structures [14].

Mucin 1 (MUC1) is a transmembrane type of mucin and it is also known by several names, such as episialin, polymorphic epithelial mucin (PEM), H23Ag, epithelial membrane antigen (EMA), cancer antigen 15-3 (CA15-3) and mucin-like carcinoma-associated antigen (MCA) [15]. It is a glycoprotein and its overexpression has a significant relationship with cancer cell proliferation, metabolism, invasion, metastasis, angiogenesis and chemoresistance [16,17]. As such, it is not only used as a biomarker but also has been defined by the National Cancer Institute as the second-best potential target out of 75 tumor-associated antigens for the development of cancer vaccine (cancer immunotherapy) [18].

Abnormal expression of MUC1 is shown including 96.7% of invasive lung cancers; 90% of pancreas, prostate, epithelial ovarian and platinum resistant tumors; 77% of primary lung cancers; 70% of breast cancers; 58% of primary lesions of prostate cancer; and in 60% of circulating tumor cells from metastatic breast, lung, pancreatic and colon cancers [19]. A low level of MUC1 expression (usually <31 U/mL) can be found in healthy human serum [20]. However, the normal MUC1 level in serum can be quite different depending on the type of assay used. In the detection tests of cancer antigens, cancer antigen 15-3 (CA15-3) levels below 25–30 U/mL are generally considered to be normal MUC1 levels in serum [21]. Therefore, levels higher than these amounts can often indicate the presence of malignancy. A 100-fold increase in the amount of MUC1 is an indication that the probability of cancer increases [22].

Biochemical analyzes such as enzyme-bound immunoassay (ELISA), radioimmunoassay, chemiluminescence immunoassay, electrochemiluminescence immunoassay developed for MUC1 determination do not allow early diagnosis due to time-consuming pretreatment requirement, high cost, qualified personnel, complex instrumentation requirement [23]. Therefore, biosensors are developed for MUC1 determination. In the literature, there are studies on nanostructured based aptasensors to develop very sensitive and selective MUC1 detection [24].

In this study, it is aimed to develop a nanomaterial based electrochemical biosensor system that provides low cost, rapid and specific analysis suitable for routine laboratory analysis and portable bedside applications as an alternative to the existing systems used for cancer diagnosis, metastasis diagnosis and cancer treatment. Nanopolymers developed by lectin affinity technique for detection of MUC1 glycoprotein were used as bioactive layer on electrochemical biosensor's electrode surface. Methacrylate based nanopolymers were synthesized using mini emulsion polymerization method in a bioreactor and derivatized

with triethoxy-3-(2-imidazolin-1 yl) propylsilane (IMEO) and Concanavalin A (ConA) lectin. Advanced characterizations were performed. The operating conditions of the sensor system have been optimized. Validation of the biosensor was performed due to statistical analysis. As part of the study, real sample blood serum was analyzed and this new method was compared with a commercially available medical diagnostic kit. The new generation nanopolymeric material has been shown to be an affordable, sensitive, reliable and rapid device.

## 2. Materials and Methods

### 2.1. Materials

2-Hydroxyethylmethacrylate (HEMA), Sodium dodecyl sulfate (SDS), Sodium bicarbonate ( $\text{NaHCO}_3$ ), Ethylene dimethacrylate (EGDMA), Sodium bisulfite ( $\text{NaHSO}_3$ ), Ammonium persulfate (APS), Polyvinylalcohol (PVA), triethoxy-3-(2-imidazolin-1 yl) propylsilane (IMEO), Concanavalin A Type 4 (Con A) were used in the synthesis of polymeric nanomaterials. They were obtained from Sigma-Aldrich (St. Louis, MO, USA). In preparation of nanoparticles shaking water bath (Mettler, Wise Bath, Germany), magnetic stirrer (Witeg Labortechnik Wisd Laboratory Instrument, Wertheim, Germany) and multiple magnetic stirrer (Witeg Labortechnik Wisd Laboratory Instrument, Wertheim, Germany), refrigerated centrifuge (Centurion K2015 R, Doncaster, England) microcentrifuge (Eppendorf Mini Spin Plus, Munich, Germany), oven Heraeus (Function Line), vortex (Dragon Lab MX-F), pH meter Neomet ISTEK (pH 240-L, Seoul, Korea), 0.1 mg sensitive scale (Kern ABS, Ballingen, Germany), sonic bath (Bandelin Sonorex RK255H, Berlin, Germany), shaker (IKA KS 125 Basic, Zevenhuizen, The Netherlands) were used as equipment.

Potassium hexacyanoferrate (III)  $\text{K}_3[\text{Fe}(\text{CN})_6]$  and potassium hexacyanoferrate (II) trihydrate  $\text{K}_4[\text{Fe}(\text{CN})_6]$ , potassium dihydrogen phosphate ( $\text{KH}_2\text{PO}_4$ ) used for electrolyte solution of biosensor were obtained from Merck (Darmstadt, Germany). Deionized ultrapure Merck Millipore Simplicity<sup>®</sup> (18.2 M $\Omega$  cm, Darmstadt, Germany) water was used in the sensor experiments. The MUC1 antigen and commercial MUC1 ELISA kit were obtained from Mybiosource (Catalog No: YLA1050HU, San Diego, CA, USA). Human serum, P2918 was purchased from Sigma-Aldrich (St. Louis, MO, USA). Alumina (0.05 micron) was used in electrode cleaning process, Ag/AgCl (containing 3M KCl in internal solution) as the reference electrode and counting electrode was platinum wire from Basi Bioanalytical System Inc. (West Lafayette, IN, USA). Basi Bioanalytical System Inc glassy carbon electrodes (West Lafayette, IN, USA) were used as working electrodes. PalmSens potentiostat (Houten, The Netherlands) as the device for which all measurements are taken. PsTrace software (Houten, The Netherlands) was used for sensor measurements, ChemBio Draw software (Perkin Elmer, MA, USA) was used for molecular interaction drawings, Edraw Max software (Shenzhen, China) was used for other schematic drawings, OriginPro (OriginLab, Northampton, MA, USA) and GraphPad Prism software (San Diego, CA, USA) were used for statistical analysis and graphs.

### 2.2. Methods

#### 2.2.1. Preparation of Nanopolymers (Synthesis, Silanization and Modification Steps)

p(HEMA) nanopolymers were synthesized with the mini-emulsion polymerization method. For synthesis, three phase system was used. First phase (aqueous phase) includes PVA, SDS,  $\text{NaHCO}_3$  in 200 mL distilled water. Then, 0.8 mL HEMA and 4.2 mL EGDMA were added to this phase as 2nd phase. The mixture was homogenized in 800–1000 rpm for 15–30 min. The 3rd phase added to the mixture was  $\text{NaHSO}_3$  and APS, then the volume was completed in 250 mL [25]. Polymerization medium was transferred to a bioreactor and the process was maintained in 40 °C, 500–700 rpm and 24 h. After 24 h, washing processes were carried out with ethanol and water for 5 times. Prepared nanopolymers were stored at +4 °C until use.

p(HEMA) nanopolymer was modified with minor changes according to [26]. In order to modify the p(HEMA) nanoparticle with IMEO, 70 mL of the p(HEMA) nanoparticle was precipitated. After separating the supernatant, it was dispersed in 15 mL of water. p(HEMA) nanoparticles in flask, 600 mL ethanol and 360  $\mu$ L IMEO distributed in 9 mL distilled water was added. It was stirred at 30 °C for 1–7 day at 200–400 rpm [26]. IMEO binds to the hydroxyl ends of p(HEMA) polymer to form p(HEMA)-IMEO modification with silane ends out. Then, washing processes were carried out with ethanol and water for 5 times.

Derivation of the prepared p(HEMA)-IMEO nanopolymers with lectin affinity chromatography ligand ConA was performed to make MUC1 specific. For this purpose, ConA would be covalently bonded to the nanopolymer surface via amino groups of IMEO. Figure 1 shows the synthesis of p(HEMA)-IMEO-ConA with the interaction between p(HEMA) and IMEO, then p(HEMA)-IMEO and ConA lectin.

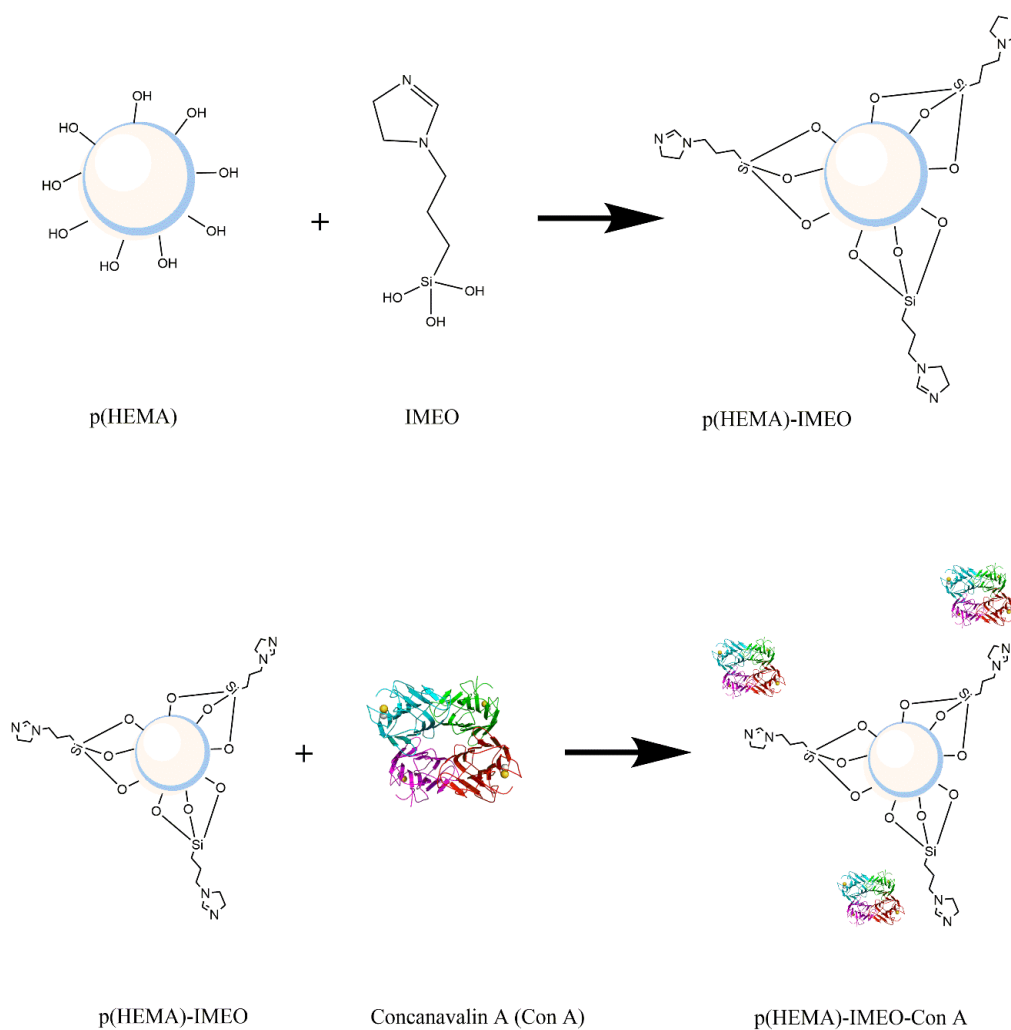


**Figure 1.** Our main strategy to develop methacrylate based MUC1 specific nanomaterial with IMEO and ConA derivatizations.

An optimization study was performed on time, pH and concentration parameters to determine ConA binding conditions. A stock solution of 0.1 mg/mL ConA (water-soluble sample diluted in 0.1 M pH 7.5 buffer) was prepared. For time effect on ConA binding, 0–120 min was tested. For pH effect on ConA binding pH 4–9 acetate, phosphate and borate buffers were used. For concentration effect on ConA binding 0.1–5 mg/mL concentration of ConA solutions were used to determine optimum concentration of ConA. Then, 100  $\mu$ L of polymer, 400  $\mu$ L of ConA solution in determined pH buffer were taken and mixed. Then,

the supernatants were read at 280 nm after centrifugation at 14,500 rpm for 35–40 min to determine the optimum parameters for ConA binding to the p(HEMA)-IMEO polymer.

### 2.2.2. Characterization of Nanopolymers

Characterization of our nanopolymers were performed with Scanning Electron Microscope (SEM), X-ray Photoelectron Spectroscopy (XPS), Atomic Force Microscopy (AFM), Fourier Transform Infrared Spectroscopy (FTIR), Zeta size and potential analysis, surface area calculations. Sensor surface was characterized due to ellipsometer and surface angle analysis.

In the sample preparation stage for SEM analysis, a 1:100 (*v/v*) diluted solution of nanopolymers was distributed over the surface of the coverslip and dried in the oven. SEM analysis of nanopolymers was performed using scanning electron microscopy (Carl Zeiss 300 VP, İzmir Katip Çelebi University Central Research Laboratories Application and Research Center, İzmir, Turkey).

For the XPS analysis, nanopolymers were precipitated at the sample preparation stage and dried in the oven after removing the upper phase. XPS analyses of nanopolymers were performed using Angle Resolution X-ray Photoelectron Spectrometry (Thermo Scientific K-Alpha, Ege University Central Research Test and Analysis Laboratory Application and Research Center, İzmir, Turkey). The applied parameters are as follows: X-ray source: Al K-Alpha Monochromatic (1486.68 eV), X-ray spot size: 200  $\mu\text{m}$ , Sampling Area: 60  $\times$  60 mm, Analyzer: 180° half-spherical analyzer-128 channel detector, Energy: 30 eV, Number of scans: 3, ARXPS angle 15°.

For the AFM analysis, the dilution solution of 1:100 ratio (*v/v*) of the nanopolymers was distributed to the surface of the coverslip and dried in the oven. AFM analyses of nanopolymers were performed using Atomic Force Microscopy (BRUKER Dimension Edge with ScanAsyst, Ege University Central Research Test and Analysis Laboratory Application and Research Center, İzmir, Turkey).

For the FTIR (Fourier Transform Infrared Spectrophotometer) measurements of nanopolymers, they were dried in the oven during the sample preparation phase. Dried nanopolymers (2 mg) for the FTIR-ATR spectrum were tested in the range of 450–4000 $\text{cm}^{-1}$  wave number. FTIR analysis of nanopolymers was performed using Fourier Transform Infrared Spectroscopy (Perkin Elmer/Spectrum Two, Ege University Institute of Nuclear Sciences, İzmir, Turkey).

The zeta size and zeta potential analyses of the synthesized p(HEMA) and p(HEMA)-IMEO and p(HEMA)-IMEO-ConA nanopolymers were performed with Nano Zetasizer (NanoZS, Malvern Instruments, Ege University Institute of Nuclear Sciences, İzmir, Turkey). For zeta size and zeta potential analysis, samples were read by diluting 1:100 (*v/v*) with distilled water.

The following equation was used to determine the surface area of synthesized p(HEMA)-IMEO-ConA nanoparticles, giving the number of particles in the 1 mL suspension [27].

$$N = 6 \times 10^{10} \times S/\pi \times \rho_s \times d^3 \quad (1)$$

where N is the number of nanoparticles in the 1 mL suspension; S, % solids; d, diameter ( $\mu\text{m}$ );  $\rho_s$  is the polymer density (g/mL).

The amount of mg nanoparticle in the mL suspension was theoretically determined using the standard mass-volume plot of the nanoparticles. The specific surface area of the synthesized p(HEMA)-IMEO-ConA nanoparticles was calculated in  $\text{m}^2/\text{g}$  using the equilibrium surface area equation.

$$\text{Surface area of sphere} = 4 \times \pi \times r^2 \quad (2)$$

( $\pi$ , 3.14; r, nanoparticle radius (m)).

For the analysis of the nanobiosensor surface, nanopolymers to be used as bioactive layer during the sample preparation phase were dropped in different volumes on a silicon

substrate cleaned in oxygen plasma for 5 min. The surface was dried in a fume hood and analysis was performed. Ellipsometer analyzes were carried out using the Ellipsometer device (Gartner, Erciyes University, Nanotechnology Application and Research Center (ERNAM), Kayseri, Turkey).

For the analysis of the nanobiosensor surface, nanopolymers to be used as a bioactive layer in the sample preparation phase were dropped on a coverslip and dried in the oven. Contact Angle analyzes (Attension Theta, Izmir Katip Çelebi University Central Research Laboratories Application and Research Center, Izmir, Turkey) were performed.

### 2.2.3. Sensor Studies

Our developed nanopolymeric material p(HEMA)-IMEO-ConA were used as a biological active surface of the biosensor's electrode. In Figure 2, recognition strategy of our nanomaterial-based biosensor was exhibited. Developed MUC1 specific p(HEMA)-IMEO-ConA nanopolymer was dropped onto electrode surface. Then, the sample that including MUC1 was dropped onto the polymer coated electrode. In each step, electrochemical measurements were performed.

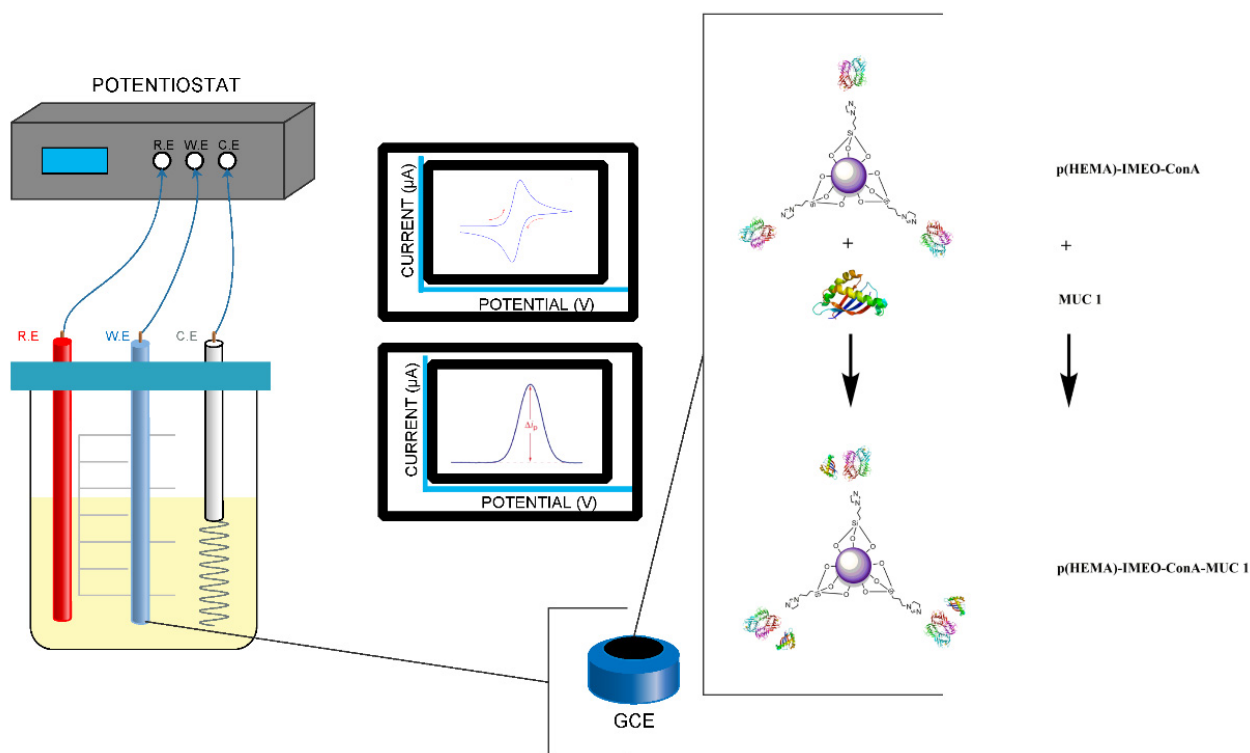


**Figure 2.** Recognition strategy of our nanomaterial-based biosensor with a schematical representation of an electrochemical biosensor.

Measurements were taken with differential pulse voltammetry (DPV) and cyclic voltammetry (CV) methods with PalmSens Potensiotat. DPV conditions were used as  $-0.4$  between  $0.6$  V with  $0.05$  V/s scan rate. Additionally, CV conditions were used as  $-0.4$  between  $0.4$  V with  $0.05$  V/s scan rate. We used  $50$  mM ferri-ferro solution as the electrolyte. In CV measurements, the decrease in the anodic potential and the increase in the cathodic potential are associated with the decrease of surface conductivity. As the thickness of the material deposited on the surface increases, the current decreases [28]. According to the DPV graph, when the nanopolymer is coated on the electrode surface, the difference on current value obtained as a result of the analysis can be interpreted that the surface is covered.

#### 2.2.4. Sensor Optimization Studies

Sensor optimization studies were performed with respect to parameters that effect MUC1 binding to the electrode. Measurements are taken by differential pulse voltammetry (DPV) and cyclic voltammetry (CV). General procedures for sensor studies were as follows:

1. Electrode cleaning (3–5 min with Alumina pasta);
2. Bare electrode was measured;
3. Determined amount of p(HEMA)-IMEO-ConA nanopolymer was dropped onto electrode surface and incubated until dry;
4. Washing was completed in ultrapure water slightly;
5. Electrode with nanopolymer was measured;
6. Determined amount of MUC1 was dropped onto p(HEMA)-IMEO-ConA binded electrode's surface and waited in determined time;
7. Washing was done in ultrapure water slightly;
8. Electrode with nanopolymer + MUC1 was measured;
9. Differences between current were calculated and graphed.

#### 2.2.5. Polymer-Electrode Binding Time

For polymer-electrode binding time parameter, p(HEMA)-IMEO-ConA nanopolymer was dropped onto the electrode's surface and incubated for 30–45–60–90–120 min. Then measurements were performed.

#### 2.2.6. Ion Effect on MUC1 Binding

Since ConA lectin, which is located at the endpoints of p(HEMA)-IMEO-ConA nanopolymer, is metalloprotein, it is thought that binding will be more effective by affecting the presence of ions during the binding to sugar groups on MUC1 [29,30]. Therefore, the effect of ions was investigated in 3 separate groups:

- Group one: 30 U/mL MUC1 solution in ultrapure water;
- Group two: 30 U/mL MUC1 was dissolved in 1 mM MnCl<sub>2</sub> and 1 mM CaCl<sub>2</sub> ion mixture;
- Group three: 2 µL of 1 mM MnCl<sub>2</sub> and 1 mM CaCl<sub>2</sub> ion mixture was added to 30 U/mL MUC1 in 4 µL ultrapure water.

5 µL of each sample was dropped onto nanopolymer coated electrodes and then waited. Then measurements were performed.

#### 2.2.7. Buffer Type Effect on MUC1 Binding

After the ion effect has been determined, to test whether there is a need for buffers to increase binding, the samples were prepared as follows:

Ultrapure water, 0.01 M phosphate-buffered saline (PBS) and 0.01 M 4-(2-hydroxyethyl)-1-piperazineethanesulfonic acid buffer (HEPES) buffer were used as pH 7.4 for ion containing buffer. A mixture of 1 mM MnCl<sub>2</sub> and 1 mM CaCl<sub>2</sub> ion was added to each buffer. MUC1 solutions were prepared at 10 U/mL concentration with these prepared buffers. p(HEMA)-IMEO-ConA nanopolymers were dropped onto the electrode surfaces (5 µL) and then incubated for 90 min. Then 5 µL of MUC1 solutions in different buffers were dropped onto the polymer and waited for 20 min. Measurements of each steps were done. Buffer type effect was determined due to differences in current.

#### 2.2.8. Ion Concentration Effect on MUC1 Binding

The samples were prepared as follows. Ultrapure water was used to pH 7.4 as the ion-containing buffer type. A mixture of 0.25–0.5–0.75–1 mM MnCl<sub>2</sub> and 1 mM CaCl<sub>2</sub> ions were added seperately. MUC1 solutions were prepared at 10 U/mL concentration with these ions including waters. p(HEMA)-IMEO-ConA nanopolymers were dropped onto the electrode surfaces (5 µL) and then incubated for 90 min. Then 5 µL of MUC1 solutions in different buffers were dropped onto the polymer and waited for 20 min. Then

measurements of each steps were done. Ion concentration effect was determined due to differences in current.

#### 2.2.9. Time Effect on MUC1 Binding

p(HEMA)-IMEO-ConA nanopolymers were dropped onto the electrode surfaces (5  $\mu$ L) and then incubated for 90 min. When 5  $\mu$ L of MUC1 solutions were dropped onto sensor surfaces, samples were kept on the electrode surface for 5–10–15–20–30–40 min. Then measurements of each steps were conducted. Time effect was determined due to differences in current.

#### 2.2.10. Nanobiosensor Characteristics and Method Validation

Nanobiosensor characteristics can be achieved by determination of several parameters and method validations. For this purpose, calibration curve, specificity, selectivity, reproducibility and storage stability determination studies were carried out. Using the prepared MUC1 calibration graph, parameters such as linearity, detection limit, determination limit, accuracy and precision parameters were calculated.

For MUC1 calibration curve, 5  $\mu$ L of 0.1–100 U/mL MUC1 solution in pH 7.4. ultra-pure was dropped on nanopolymers bounded carbon electrode and measurements were taken after 20 min. Graphics were obtained from the current differences obtained as a result of DPV measurements.

p(HEMA) and p(HEMA)-IMEO-ConA nanopolymer were compared for specificity testing. And general procedure was performed with these nanopolymers seperately. Nanopolymers were dropped onto electrode surfaces and incubated for 90 min. Then 5  $\mu$ L of 30 U/mL MUC1 in 1 mM MnCl<sub>2</sub> and 1 mM CaCl<sub>2</sub> was added and waited for 20 min. Then measurements were taken and speticificity was determined due to the differences in current.

For the selectivity assay, p(HEMA)-IMEO-ConA nanopolymers were dropped onto the electrode surfaces (5  $\mu$ L) and then incubated 90 min. Then, 0.05 mg/mL mannose, 0.05 mg/mL Immunoglobulin G (IgG) and 10 U/mL Cancer Antigen 125 (CA125) and 0.05 mg/mL Bovine Serum Albumin (BSA) were compared with 10 U/mL MUC1. 5  $\mu$ L of each of the samples were dropped onto the polymer seperately, then waited for 20 min. Measurements were taken and selectivity of the developed nanopolymer were determined due to the differences in current.

Prepared electrodes were stored at +4 °C for 5 days, 10 days, 20 days, 30 days and 60 days. At the end of each time period, the samples were dropped (5  $\mu$ L of 10 U/mL MUC1, 25 °C, 20 min) and measurements were taken.

For reproducibility tests, measurements were taken in different times and differences in current were calculated with using calibration curve as U/mL. Experiments were repeated 6 times and performed in optimum conditions that are determined in previous studies.

Validation studies of our sensor were carried out due to parameters of linearity, limit of detection (LOD), limit of quantification (LOQ), accuracy, RSD%, confidence limit and sensitivity. For linearity, R<sup>2</sup> value of MUC1 calibration curve was used.

Linear regression is a statistical method for calculating the value of a dependent variable from an independent variable. This method measures the relationship between two variables [31]. Here, we used the linear regression model in order to determine the concentration of MUC1 effect on current changes. This graph was used as the calibration curve. The calibration curve of target biomarker is used to calculate the sensitivity parameter. The linear calibration curve equation is defined in  $y = a + bx$  equation. LOD and LOQ were calculated with Equations (3) and (4) as follows:

$$\text{LOD} = 3 \times \frac{S_a}{b} \quad (3)$$

$$\text{LOQ} = 10 \times \frac{S_a}{b} \quad (4)$$

where  $S_a$  is the standard deviation of the response and  $b$  is the slope of the calibration curve [32].

Precision of a parameter of the degree of closeness measurements among individual test results when the procedure is applied repeatedly to multiple samplings. And it is related with relative standard deviations (RSD) [33,34]. Accuracy is another parameter of analytical methods that is related with degree of agreement of test results generated by the method to the true value [34]. Recovery, relative standard deviation (RSD%) and confidence limit were calculated with the following formulas and Grubbs' test was applied. Grubbs' test is applied when the testing the null hypothesis that a suspected value is an outlier versus the alternative hypothesis that the suspected value is not an outlier. It is easy to apply and operated using the mean and standard deviation of the data [35].

$$R = \frac{C}{C_{ref}} \times 100 \quad (5)$$

$C$  = known concentration of analyte,  $C_{ref}$  = average of analyte concentrations found as a result of reproducibility testing [36].

Relative Standard Deviation% (RSD%) value was calculated with Equation (6).

$$\text{RSD}\% = \frac{S}{\text{average value}} \times 100 \quad (6)$$

$S$  = standard deviation.

Student's  $t$ -test is a common method when testing hypotheses about the mean of a small sample drawn from a normally distributed population when the population standard deviation is unknown. The main focus of  $t$ -tests is on describing a situation such as: (a) Mean/proportion in one sample, (b) mean/proportion in two unrelated samples, (c) mean/proportion in two related samples, (d) correlation coefficient and (e) regression coefficient [37]. In this study we used  $t$ -test for the confidence limit calculation and reference kit comparison.

Confidence limit (CL) calculation is another way of determining the accuracy of an analysis [38]. Equation (7) is used for confidence limit calculation.

$$\text{Confidence limit (CL)} = \text{average value} \mp t \frac{S}{\sqrt{n}} \quad (7)$$

$n$  = the number of repetitions,  $t = (n - 1)$ .

$t$  value read from the table,  $S$  = standard deviation.

To determine the accuracy of the method, Grubbs' test was calculated using GraphPad with the Equation (8) formula below.

$$Z = \frac{|\text{average value} - \text{measured value}|}{S} \quad (8)$$

Using the Grubb table, the critical  $Z$  value determined for the number of samples is compared with the calculated  $Z$  value with the Equation (9) formula. If the calculated  $Z$  value is less than the critical  $Z$  value, it is stated that the precision of the analysis is high [39].

Reality parameter is determined by systematic error calculation ( $t$ ).

$$t = \frac{(X_{\text{calculated}} - X_{\text{CRM}}) \times \sqrt{n}}{S} \quad (9)$$

$X_{\text{calculated}}$ , average of analyte concentrations obtained as a result of reproducibility testing,  $X_{\text{CRM}}$  = known concentration of analyte,  $n$  = number of repetitions,  $S$  = standard deviation.

The reality is calculated by examining whether there is a significant difference between the systematic error value calculated with the formula above and the actual value calculated by doing *t*-tests [40].

#### 2.2.11. Real Samples Experiments

The general procedure for real sample testing were performed and repeated 3 times. Samples were prepared as follows:

Samples in different concentrations prepared in blood serum with a serial dilution (0.5–1–5–10–50–100 U/mL) and dropped into the electrode surface (5 µL, 25 °C, 20 min). After each step, cleaning is performed with ultra-pure water and measurements are taken by differential pulse voltammetry (DPV) and cyclic voltammetry (CV). For the calculations, the equation in the MUC1 calibration graph was used and the U/mL concentrations of the samples analyzed at the end of the experiment were determined.

#### 2.2.12. Reference Kit

As a reference kit, MUC1 ELISA kit was used. Standard procedure in kit was performed. OD values were read in 450 nm and calibration curve was plotted. Calibration graph was prepared with standard solutions prepared at 0.25–8 ng/mL concentration. MUC1 in different concentrations (0.5, 1, 5, 10, 50, 100 U/mL) prepared in the blood serum (Human Serum, P2918, SIGMA ALDRICH) and used for comparison test.

The results obtained within the scope of the comparison study with the reference method were checked for accuracy by performing a *t*-test. For this purpose, a comparison was made with the *t* test calculated using the Equations (10) and (11) [40].

$$t = \frac{(\overline{X}_1 - \overline{X}_2)}{s \sqrt{\frac{1}{n_1} + \frac{1}{n_2}}} \quad (10)$$

$$s^2 = \frac{(n_1 - 1)s_1^2 + (n_2 - 1)s_2^2}{n_1 + n_2 - 2} \quad (11)$$

$\overline{X}_1 - \overline{X}_2$  : difference of average values taken in measurements.

*s*: standard deviation value.

*n*: number of samples.

### 3. Results

#### 3.1. Optimization of Synthesis of Nanopolymers

Optimization of ConA binding to p(HEMA)-IMEO nanoparticles were carried out with respect to time, pH and concentration parameters with three repeated experiments. In the Figure 3A, optimum time for ConA binding to p(HEMA)-IMEO was determined as 60 min and Q value was calculated as 134.60 µg/g polymer. As we expected, ConA binding to p(HEMA) was less than p(HEMA)-IMEO.

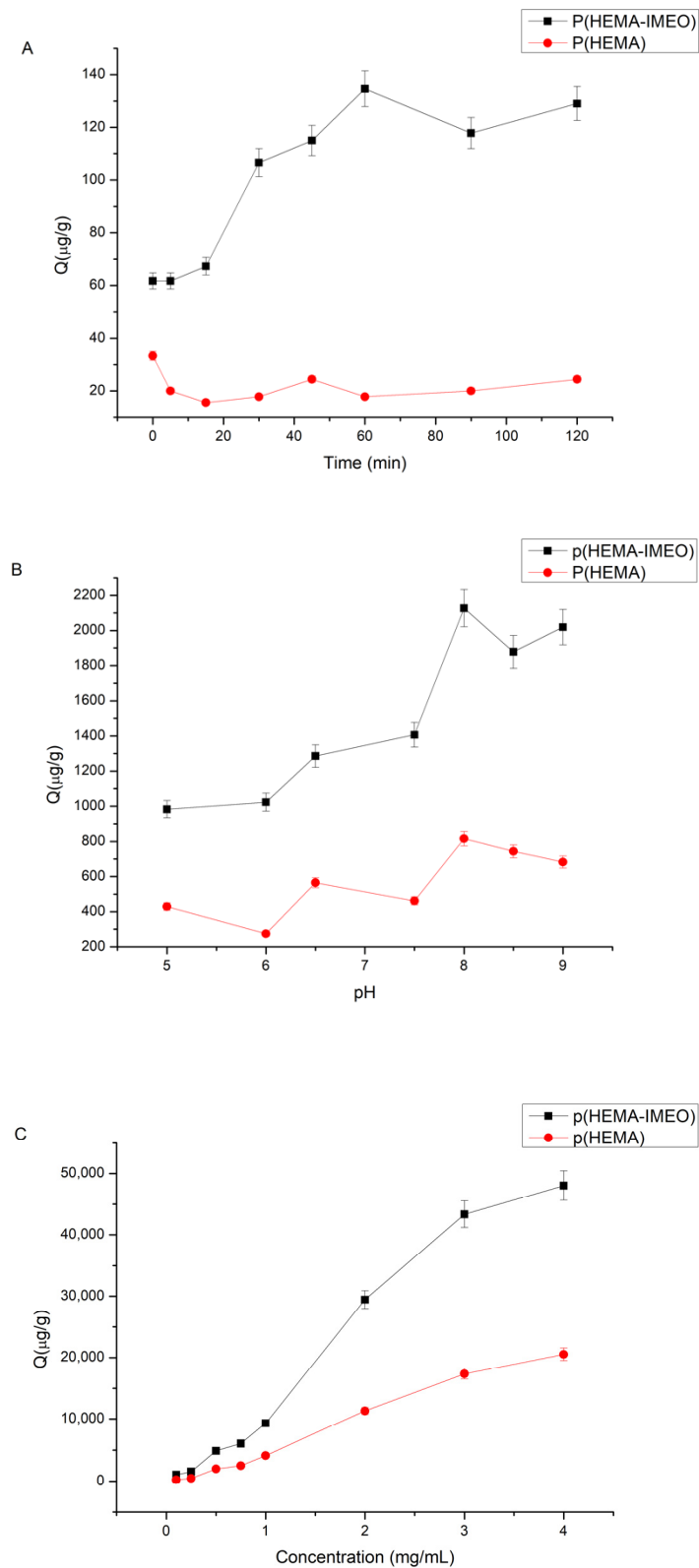


**Figure 3.** Parameter's effect on ConA binding to developed nanopolymer: **(A)** Time effect on ConA binding to p(HEMA)-IMEO nanopolymer (ConA: 0.1 mg/mL, 0.1 M pH 7.5 phosphate buffer), **(B)** pH effect on ConA binding to p(HEMA)-IMEO nanopolymer (time: 60 min; 0.1 mg/mL ConA; pH 4.0, pH 5.0 0.1 M acetat buffer pH: 6.5–7.5–8 0.1 M phosphate buffer; pH 9.0–10.0 0.1 M borate buffer), **(C)** Concentration effect on ConA binding to p(HEMA)-IMEO nanopolymer (time: 60 min; pH 8.0 0.1 M phosphate buffer).

In Figure 3B, optimum pH for ConA binding to p(HEMA)-IMEO was determined as pH 8.0 and Q value was calculated as 2126.8  $\mu\text{g/g}$  polymer. As we expected, ConA binding to p(HEMA) was less than p(HEMA)-IMEO.

In Figure 3C, optimum ConA concentration for ConA binding to p(HEMA)-IMEO was determined as 4 mg/mL and Q value was calculated as 48,038.7  $\mu\text{g/g}$  polymer. As we expected, ConA binding to p(HEMA) was less than p(HEMA)-IMEO.

Summarily, optimization parameters were determined as 60 min, 4 mg/mL concentration and pH 8.0 0.1 M phosphate buffer.

### 3.2. Characterization of Nanopolymers

#### 3.2.1. SEM Analysis

In Supplementary Materials File Figure S1, nanopolymers can be seen with spherical shapes and approximately 80 nm sizes.

#### 3.2.2. XPS Analysis

XPS analysis results of p(HEMA)-IMEO nanopolymers are examined, N% content is determined as 1.05 (0.029 mg/mL polymer) and Si% content is determined as 1.16 (0.032 mg/mL polymer). When compared with the XPS results of p(HEMA), it was proved that the modification was successful with the presence of silisyum and nitrogen which had not been in the structure and in the result of analysis before and IMEO was included in the structure.

#### 3.2.3. AFM Analysis

Ra is the center-line mean or arithmetic mean and Rq is the root mean square, and Rmax is the maximum surface roughness [41]. Ra is typically used to define the roughness of modified surfaces. It is useful for detecting general differences in overall profile height characteristics and monitoring an established production process [42]. As shown in Table 1, Ra value of p(HEMA)-IMEO nanopolymer is greater than Ra value of p(HEMA) nanopolymer. In this case, surface modification of p(HEMA) nanopolymer with IMEO increased surface roughness. The Rq value is more sensitive to higher peaks and valleys depending on the square of amplitude in the calculation of Ra [43]. The increase in Rq value can also be associated with surface modification. Looking at the value of Rmax, we can say that p(HEMA)-IMEO has a rougher surface than p(HEMA) [44]. From the AFM results it can be said that modification and derivation of p(HEMA) nanomaterials was resulted with changing in surface topology and porosity (Supplementary Material File Figure S2).

**Table 1.** AFM Results.

Nanopolymer	Ra	Rq	Rmax
p(HEMA)	7.14 nm	14.7 nm	194 nm
p(HEMA)-IMEO	0.0196 $\mu\text{m}$	0.0235 $\mu\text{m}$	0.145 $\mu\text{m}$

#### 3.2.4. FTIR Analysis

As can be seen from the FTIR spectrum (Supplementary Materials File Figure S3), -OH bands around  $3500\text{ cm}^{-1}$  in p(HEMA) nanoparticles became prominent. FTIR analysis shows that modification and derivation of p(HEMA) nanomaterial was successful due to specific bands of silanization agent and lectin. When the FTIR spectra is shown, p(HEMA)-IMEO nanopolymer characteristic is about  $1721\text{ cm}^{-1}$  carbonyl (C=O) band, vibration bands belonging to methyl groups around  $2958\text{ cm}^{-1}$ . Si-O-C stresses specific to the presence of IMEO are seen at  $1245\text{ cm}^{-1}$  [45]. The tension bands of the Si-O-Si bond were observed at  $1145\text{ cm}^{-1}$ . C-O vibration voltages are observed around  $1245\text{ cm}^{-1}$ . Amide I tensile bands are observed at  $1636\text{ cm}^{-1}$  as a proof that ConA has entered the structure. The band at  $1522\text{ cm}^{-1}$  can be interpreted as belonging to tyrosines in ConA [46].

### 3.2.5. Zeta Size and Potential Analysis

Average particle size was between 120 and 190 nm and PDI value was 0.375 (Supplementary Materials File Figure S4). According to Zeta size and PDI values, modifications and derivatizations made on p(HEMA) appear to cause minor changes in particle size. Since PDI values are below 1, it can be said that it is in homogeneous distribution for particle sizes. The difference between the size data obtained after SEM analysis and the zeta size data is related to the swelling behavior of the suspended particles and the Brownian motion. Zeta is a situation where you are expected to have higher results than SEM results [47].

According to Supplementary Materials File Figure S5, zeta potential average value of p(HEMA)-IMEO-ConA was determined as  $-31.27$  mV and it is well known that potential values higher than  $+30$  mV or lower than  $-30$  mV permits a basically stable suspension [48]. So, as can be seen from the zeta potential values, p(HEMA)-IMEO-ConA is more stable than p(HEMA).

### 3.2.6. Surface Area Calculations

According to the SEM analysis of p(HEMA) nanopolymer, the average size of the nanoparticle was taken as 79.35 nm. Specific surface area of p(HEMA) with dry polymer mass = 0.00685 g/mL was found to be  $1123.48$  m<sup>2</sup>/g specific surface area. Nanoparticle average size of p(HEMA)-IMEO-ConA nanoparticles was taken as 75.635 nm according to SEM analysis. The specific surface area of p(HEMA)-IMEO-ConA with dry polymer mass = 0.00062 g/mL was found to be  $13583.73$  m<sup>2</sup>/g specific surface area.

As the nanoparticle size decreases, the percentage of surface atoms/molecules increases significantly. Nanoparticle isoelectric point and surface reactivity depend on particle size. In addition, as the size changes, the particle electronic structure, surface defect density and surface absorption zones also change [49].

### 3.2.7. Ellipsometer Analysis

Different volumes of p(HEMA)-IMEO-ConA nanopolymer were used for ellipsometer analysis via calibration curve of thickness. Table 2 shows that, measurements and standard deviation values. In 12.5 and 15  $\mu$ L, standard deviations are too high. In 2.5  $\mu$ L, the volume is too small and the electrode surface is not fully coated and the risk of pipetting error is high. The sample placed in a volume of 5  $\mu$ L covers the electrode surface completely and the standard deviation is within acceptable limits. Therefore, the amount of nanopolymer to be placed on the electrode surface was chosen as 5  $\mu$ L in order to avoid wasting excess polymer.

**Table 2.** Ellipsometer measurements and standard deviations.

Polymer Volume ( $\mu$ L)	2.5	5	7.5	12.5	15
p(HEMA)-IMEO-ConA	239.61	614.09	1313.66	3200.85	6358.60
Standard deviation	0.09	0.28	0.12	5.59	11.21

### 3.2.8. Surface Angle Analysis

As a result of the analysis, the contact angle of the p(HEMA) nanopolymer was  $39.53^\circ$ , the contact angle of the p(HEMA)-IMEO nanopolymer was  $52.25^\circ$  and the contact angle of the p(HEMA)-IMEO-ConA nanopolymer was  $39.008^\circ$  (Table 3).

**Table 3.** Surface angle analysis results (ST [mN/m]).

Polymer	p(HEMA)	p(HEMA)-IMEO	p(HEMA)-IMEO-ConA
Mean (ST[mN/m])	39.53	52.25	39.008
Standard deviation	1.25	1.59	1.87

Hydrophilic surface is the case that has a low water contact angle and the water droplet spreads or wet the surface. Hydrophobic surfaces are surfaces with a high-water contact angle, where the water droplet “sits” on the surface. In this case, we can say that the hydrophobicity of the nanopolymer increased with the participation of IMEO in the structure, while the hydrophobicity decreased again with ConA binding. However, we can say that all three nanopolymers are wet because the contact angle value is less than  $90^\circ$  [50].

### 3.2.9. CV Analysis

The CV measurements taken at each stage of the experiments (As a bare electrode, after p(HEMA)-IMEO-ConA nanopolymer binding and MUC1 binding) were combined under optimum conditions obtained as a result of the trials. Additionally, it was investigated whether MUC1 concentrations are changed, the current values taken from the CV analysis also change proportionally. It can be said that the developed nanobiosensor system responds sensitively to MUC1 biomarker at different concentrations (Supplementary Materials File Figure S6).

### 3.3. Optimization of Sensor Parameters

Several parameters of binding process such as polymer-electrode binding time, ion effect on binding, ionic concentration effect, calibration curve and response time were determined and optimized due to DPV analysis results.

#### 3.3.1. Polymer-Electrode Binding Time

Polymer-electrode binding time was determined as 90 min due to Figure 4 and more waiting time is thought to be unnecessary.

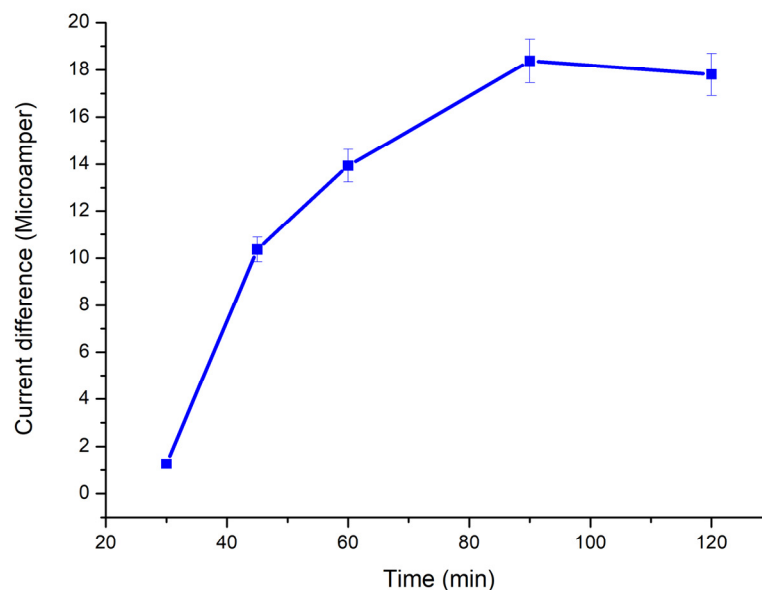


**Figure 4.** Time effect on nanopolymer binding on electrode surface (5  $\mu$ L p(HEMA)-IMEO-ConA nanopolymer, 25  $^\circ$ C, 30–45–60–90–120 min).

#### 3.3.2. Ion and Ionic Concentration Effect on Binding

When the effect of ion to MUC1 binding to p(HEMA)-IMEO-ConA nanopolymer over electrode surface is examined, it is seen that MUC1 dissolved in ion-containing water creates the most current change (Figure 5A). Therefore, during the studies, readings were made by adding MUC1 into the ion mixture before dropping it on the sensor’s surface, obtaining a pre-mixture and then dropping it on the sensor surface.

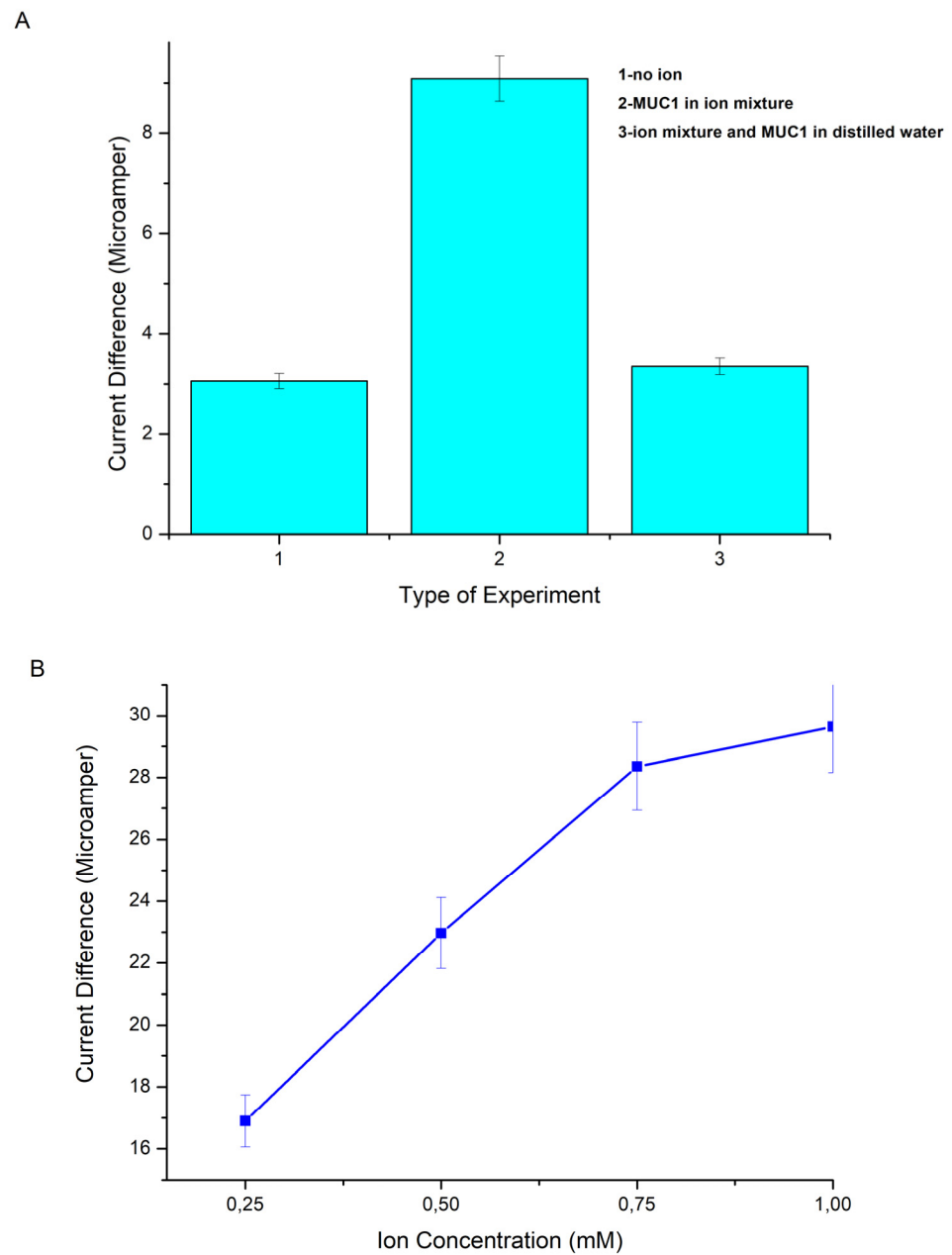


**Figure 5.** Ion and ion concentration effect on binding of MUC1 to developed nanopolymer: (A) Ion Effect on Binding of MUC1 to p(HEMA)-IMEO-ConA nanopolymer (5  $\mu$ L p(HEMA)-IMEO-ConA nanopolymer, 25  $^{\circ}$ C, 90 min, 10 U/mL MUC1, 1 mM ion mixture, 25  $^{\circ}$ C, 20 min), (B) Ion Concentration Effect on MUC1 Binding (5 $\mu$ L p(HEMA)-IMEO-ConA nanopolymer, 25  $^{\circ}$ C, 90 min, 10 U/mL MUC1, 25  $^{\circ}$ C, 20 min).

It was experimentally confirmed that MUC1 binding was increased in the presence of ions, and it was observed that the current change reached saturation at the ion concentration of 1 mM (Figure 5B). Therefore, 1 mM ion mixture (1 mM  $\text{MnCl}_2$ , 1 mM  $\text{CaCl}_2$ ) was used in the experiments.

### 3.3.3. MUC1 Calibration Curve

When the results obtained from the experiment are examined, the determination range can be expressed linearly between 0.1 and 100 U/mL (Figure 6). Additionally, when the normality test was applied, the data was not significantly drawn from a normally distributed population since it is lower than 0.05 (for concentration probability < W 0.00168).

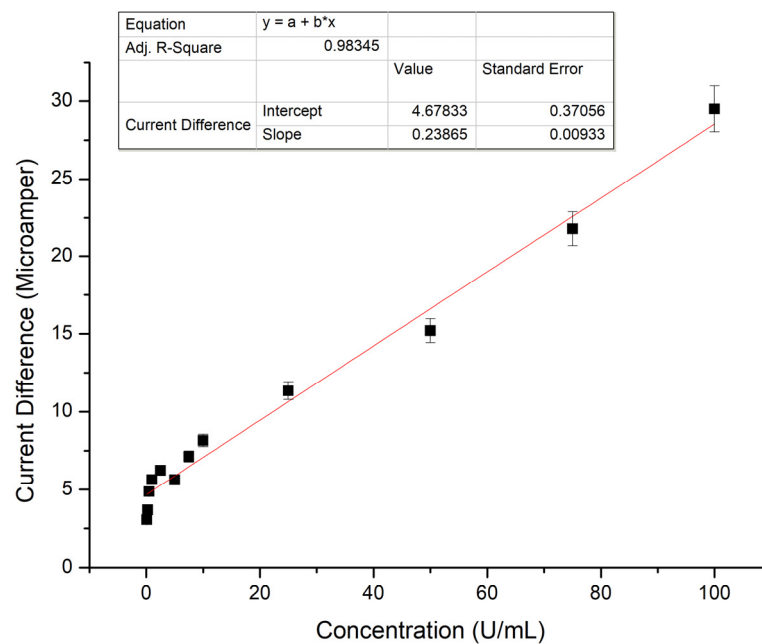


**Figure 6.** MUC1 concentration graph (5  $\mu$ L p(HEMA)-IMEO-ConA nanopolymer, 25  $^{\circ}$ C, 90 min, 0.1–0.25–0.5–1–2.5–5–10–50–100 U/mL MUC1 + 1 mM MnCl<sub>2</sub>, 1 mM CaCl<sub>2</sub> ion mixture, 25  $^{\circ}$ C, 20 min).

The determination range appears to cover a wide range. Since the value of 31 U/mL, which is a critical value for the disease, is within the determination range, it is considered that individuals with suspected disease can be accurately distinguished from healthy individuals by this method.

In the literature, surface imprinted carbon electrodes were modified with multi-walled carbon nanotubes (MWCNT) to prepare aptamer sensors for MUC1 and an impedimetric response in the range of 0.1–2 U/mL was obtained [51]. In another study, using a magnetic particle modified capacitive sensor, a carcinoembryonic antigen (CEA), human epidermal growth factor receptor (hEGFR) and cancer antigen 15-3 (CA15-3, MUC1) were analyzed and CEA and hEGFR were analyzed at 5 pg/mL to 1 ng. CA15-3 was determined with a limit of 10 U/mL in the range of 1–200 U/mL with high specificity [52]. In another study, the immunosensor with a high conductivity graphene modified electrode exhibited significantly increased electron transfer and high sensitivity to CA 15-3. This novel immunosensor worked well over a wide linear range of 0.1–20 U/mL with a low detection limit of 0.012 U/mL [53]. In this case, our system can measure with high R<sup>2</sup> value in the range of 0.1–100 U/mL and our system can compete with the examples in the literature can be interpreted.

### 3.3.4. MUC1 Response Time

p(HEMA)-IMEO-ConA nanopolymers have high potential for determination of MUC1 with short time. Response time was determined as 20 min (Figure 7).

In the study of Ding et al., it was reported that the graphene oxide and carbon dots functionalized with aptamer can recognize MUC1 as fluorescence in 60 min [54]. In another study shows that MUC1 can be analyzed within 15 min with enzyme based fluorescent aptasensor method developed by Zhang et al. [55]. It is seen that the response time of the nanopolymer we developed to MUC1 is competitive with the examples in the literature.

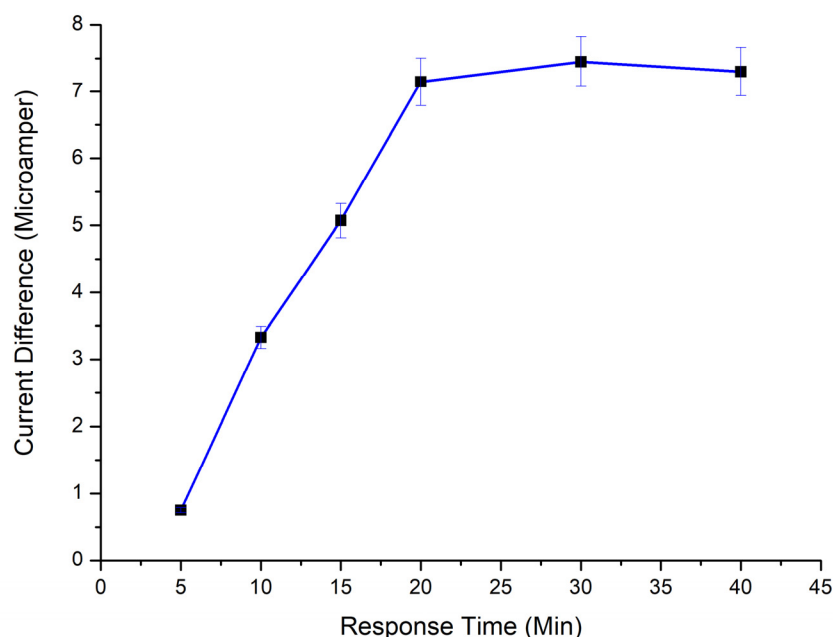


**Figure 7.** Time effect on MUC1 binding to nanopolymer on electrode surface (5  $\mu$ L np (1:100 dilution), 90 min; 10 U MUC 1 in pH 7.4 ultra pure water).

When the electrochemical sensor studies developed to recognize MUC1 are examined, it is seen that the response times vary between 20 and 60 min. Therefore, it can be interpreted that the optimized 20 min value is competitive with the examples in the literature.

### 3.4. Nanobiosensor Characteristics and Method Validation

Linearity of our method was 98.5% as the  $R^2$  value of the MUC1 calibration curve.

LOD was calculated as 13.74 U/mL and LOQ was calculated as 45.81 U/mL. Our results are close to Altintas et al. developed system [52]. However, there are also studies with a lower detection limit in the literature. For example, Li et al. developed a system that can determine the MUC1 saliva and its LOD value is 0.012 U/mL [53]; and other studies from Hong et al. have LOD of 0.64 U/mL [56].

Accuracy of the method was tested due to  $t$ -test ( $n = 6$ ).  $t_{\text{calculated}} = 2.2360$  and  $t_{\text{critical}} = 2.57$  ( $p = 0.05$  for  $n - 1 = 5$ ). Since  $t_{\text{calculated}} < t_{\text{critical}}$ , it can be interpreted that the measurements are true [57].

As shown by Grubbs' test on the online tool of GraphPad Prism ( $n = 6$ ), since the calculated values are smaller than the critical values, there is no inconsistency in the values (Supplementary Materials File Figure S9). The confidence limit of the measurements was  $10.89 \pm 0.47$  for  $p = 0.05$ .

The sensitivity value is the slope of the equation for the calibration curve. In other words, the sensitivity of the developed method is 0.2386 U/mL.

It resulted as our lectin-based nanomaterial is 4.5-fold specific to MUC1 than non-modified HEMA based one (Figure 8A). It can be said that our modification process was successful in order to specify nanopolymeric material for MUC1 due to silanization and lectin affinity.

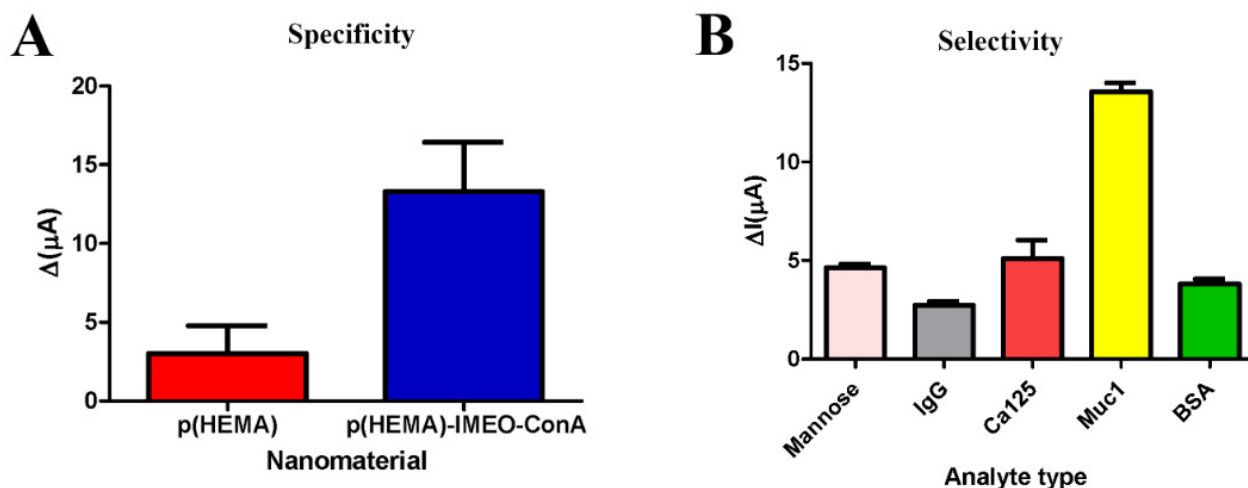


**Figure 8.** Specificity and selectivity assays of developed nanopolymer: (A) Specificity analysis (5  $\mu$ L np (1:100 dilution), 90 min; 10 U/mL MUC1 in pH 7.4 ultra pure water, 20 min), (B) Selectivity analysis (5  $\mu$ L np (1:100 dilution), 90 min; 10 U/mL MUC1 in pH 7.4 ultra pure water, 10 U/mL CA125, 0.05 mg/mL BSA, 0.05 mg/mL IgG, 0.05 mg/mL mannose, 20 min).

p(HEMA)-IMEO-ConA is 3.5-fold selective for MUC1 rather than others due to its variety of sugar parts (Figure 8B).

According to the results of the storage stability test, the current values obtained were converted to concentration with the help of the equation obtained in the concentration curve. It can be interpreted that these electrodes have a high stability in the first 5 days but decreased over time. The measured value taken on the 5th day decreased by 2%, 8.5% on the 10th day, 16% on the 20th day, 21% on the 30th day and 36.5% on the 60th day. It can be interpreted that the electrodes are stable since the prepared electrodes still have 63% activity after 60 days (Supplementary Materials File Figure S7).

Liu et al. reported molecularly imprinted polymer-based electrochemical sensors for 2,4-DCP determination in 2016. In the study, a 7% decrease in electrode stability was observed within 2 weeks [58]. Kiss et al. were developed molecularly imprinted polymer-based electrochemical sensor for the determination of dopamine in 2016. The stability of the electrodes decreased by 2% after 1 week, 6% after 2 weeks, and about 18% after 1 month [59]. It can be said that the results obtained as a result of our study can compete with the polymeric based electrochemical sensor samples in the literature.

According to these calculations, the mean value was 10.89 U/mL, recovery value (R) was 91.82% and RSD value was 4.13%. There is no significant difference between the actual value and the method is considered to have the potential to make the correct determination (Supplementary Materials File Figure S8).

As a summary, our developed nanobiosensor characteristics are listed in Table 4.

**Table 4.** Our sensor characteristics.

Sensor Characteristics	Obtained Values
LOD	13.74 U/mL
LOQ	45.81 U/mL
Response time	20 min
Sensitivity	0.2386 U/mL
Linear Range	0.1–100 U/mL
Recovery	91.82%
RSD%	4.13%
Confidence level	10.89 $\pm$ 0.47 U/mL

### 3.4.1. Real Samples Experiment

Due to Table 5, it can be said that the real serum sample trials of the developed system are successful with low error% values. The system developed in this way has the potential to be used in clinical research and diagnostic applications.

**Table 5.** Experimental results with known antigen samples.

Known Antigen Samples (U/mL)	Measured Antigen (U/mL)	Error (U/mL)	Error%
0.5	0.473	−0.026	5.332
1	1.027	0.027	2.728
5	5.140	0.140	2.811
10	10.675	0.675	6.758
50	49.704	−0.295	0.591
100	98.989	−1.010	1.010

### 3.4.2. ELISA Test

The measurement range of the ELISA kit which was used (Catalog No: YLA1050HU) is 0.05–15 ng/mL, sensitivity is 0.024 ng/mL. When the Supplementary Materials File Figure S10A is examined with normality test, at the 0.05 level absorbance values were drawn from a normally distributed population (probability < W 0.42258). For this reason, this line was not linearized.

And when Figure S10B is examined, it is seen that there was a high correlation between the results obtained with the developed biosensor and the results obtained with MUC1 ELISA kit (Table 6).

**Table 6.** Comparison of nanobiosensor and ELISA kit.

Concentration (U/mL)	Obtained Results from Nanobiosensor (U/mL)	Obtained Results from ELISA Kit (U/mL)	Standard Deviation
0.5	0.47	0.47	0.08
1	1.03	1.40	0.18
5	5.14	5.23	0.04
10	10.68	10.68	0.0005
50	49.70	50.51	0.4
100	98.99	100.26	0.63

For the *t*-test made using the values obtained according to the measurements taken by the reference method ( $n_{\text{total}} = 9$ ), the calculated value was found to be 0.53. The  $t_{\text{critical}}$  value for ( $n_{\text{total}} - 2$ ) can be drawn from the table as 2.36. It can be interpreted that there is no significant difference between the two methods since  $t_{\text{calculated}} \leq t_{\text{critical}}$  by the statistical analysis performed between the developed kit and the ELISA kit results made by dropping the patient's blood.

## 4. Discussion

While preparing the p(HEMA)-IMEO-ConA nanoparticles used in the developed system, the p(HEMA) nanoparticles were synthesized by the mini emulsion polymerization method, followed by silanization with IMEO. The ConA lectin was used for modifying the p(HEMA)-IMEO nanopolymer according to the lectin affinity method. As a result of the optimization studies, optimum ConA binding conditions were determined as pH 8.0, 0.1 M phosphate buffer, 1 h adsorption time, 4 mg/mL ConA concentration. When the XPS analysis results of p(HEMA)-IMEO nanoparticles are examined, N% content is 1.05 (0.029 mg/mL polymer) and Si% content is 1.16 (0.032 mg/mL polymer). Compared with the XPS results of p(HEMA), it has been proved that the modification was successful with the presence of silica and nitrogen, which were not previously in the structure, and that the

IMEO joined the structure successfully. Thus, the participation of IMEO and ConA in the structure were confirmed by FTIR and XPS analysis.

When the characterization data of the prepared p(HEMA)-IMEO-ConA nanoparticles were examined, it was seen that the nanoparticles were obtained in spherical morphology between 70 and 80 nm sizes. AFM analysis proved that porosities of nanoparticles were changed. Nanoparticle dimensions and surface loads were determined by zeta size and zeta potential analyzes. The specific surface area of p(HEMA)-IMEO-ConA nanoparticles was calculated as 13583.73 m<sup>2</sup>/g. Characterization of the sensor surfaces were completed with the ellipsometer and contact angle analysis. The amount of polymer to be placed on the surface was determined as 5 µL by ellipsometer analysis. Modifications made according to the contact angle analysis have been shown to cause differences in the morphological, chemical and physical properties of nanoparticles.

As a result of the DPV measurements, the optimum time for the binding of p(HEMA)-IMEO-ConA nanopolymer to the glassy carbon electrode surface is 90 min. The response time for MUC1 binding to the nanopolymer was determined as 20 min, and the linear measurement range was determined as 0.1–100 U/mL. Within the scope of the specificity study, p(HEMA)-IMEO-ConA nanoparticles were determined to be 4.5 times more specific than p(HEMA) nanopolymer. In the selectivity study, it was determined that p(HEMA)-IMEO-ConA nanopolymer was approximately 3.5 times more selective than the molecules with other recognition capacity (mannose, IgG, CA-125, BSA) to the MUC1 glycoprotein.

Stability experiments exhibited that the electrodes are stable since the prepared electrodes still have 63% activity after 60 days.

It can be seen that the developed system can measure MUC1 in the real sample with low error values. As a reference method, performance comparison was made with the MUC1 ELISA kit, and there is a correlation between the results (Supplementary Materials File Figure S10A,B). Since there was no statistically significant difference between the result of the developed kit and the result of the ELISA test, the success of the kit that we developed was proved. It is seen that the developed nanopolymeric material-based electrochemical biosensor has the potential to be used as a system to determine MUC1 for cancer diagnosis/prognosis and monitoring, metastasis detection and the success of chemotherapy.

Literature review and comparison were made with our study in terms of LOD, response time, linear range, recovery and RSD% values. It can be seen as listed as in Table 7. In line with all these data, the current study that can compete with the examples in the literature and can provide cheaper and faster measurement, as cost-effective products are used. In addition, since a sensor made with a similar affinity method is not found in the literature, it can be described as a unique study for MUC1 determination. In general, the study stands out with its reasonable cost, a short response time of 20 min, wide measurement range and the ability to receive a response in a statistically similar correlation with the reference kit.

**Table 7.** Comparison of electrochemical sensors for MUC1.

Electrochemical Sensors	LOD	Response Time	Linear Range	Recovery	RSD%	References
Rauf et al. 2018	0.04 U/mL	60 min	0.1–2 U/mL	96–96.67%	4.2%	[60]
Altıntaş et al.2012	10 U/mL	-	1–200 U/mL	-	-	[52]
Li et al. 2013	0.012 U/mL	-	0.1–20 U/mL	104.2%	1.82%	[53]
Hong et al. 2009	0.64 U/mL	-	2.0–240 U/mL	101.4%	-	[56]
This study	13.74 U/mL	20 min	0.1–100 U/mL	91.82%	4.13%	-

The patent research for this study was made using <http://www.espacenet.com>, (accessed on 18 Jan 2021) as the database. During the patent search, “CA 15-3 biosensor” was used as keywords. In the patent number WO2018011474A1, a lectin-based cancer diagnosis system has been developed. The current system is to determine the presence of CEA, CA 19-9 and CA 15-3, which are used as biomarkers for breast, colorectal and

pancreatic cancer. Macrophage galactose type lectin (MGL) was used in the system, and the recognition of biomarkers was carried out with an ELISA-like operating principle over HRP-labeled antibody. In the presented thesis, an electrochemical biosensor system is developed with lectin-based nanomaterial surface electrodes that can detect MUC1 (CA 15-3) for cancer types.

When the literature and patent studies are examined, the originality and patent potential of the system developed within the scope of this study can be seen. Since there is no similar study or patent in terms of material strategy and application, the nanobiosensor system developed within the scope of the thesis is a first in the literature. The nanomaterial-based electrochemical biosensor system, developed for cancer diagnosis/prognosis and monitoring, has the potential to be a product that will contribute to the domestic and national economy, allowing rapid analysis. After the necessary stabilization studies, it is possible to be combined with artificial intelligence supported applications and transform into a system that can provide information to patients, relatives and healthcare personnel. The developed system can offer a comfortable life to the patient, contribute to the health economy at a high cost as a domestic production, prevent unnecessary drug use, imaging and analysis in cancer follow-up.

## 5. Conclusions

It is possible to use the current study as a biosensor for detection of MUC1 levels in potential cancer patients or already patients with these encouraging results. Our recognition strategy that is based lectin affinity without using aptamers or antibodies is the first study in the literature. However, it is clear that this study can be still developed in terms of LOD or response time parameters. If it is desired to measure at lower LOD values, experiments can be performed using a specific lectin for MUC1-C subgroups such as C-type lectin, galactose type lectin or other plant derived lectins instead of Concanavalin A. There are some studies about MUC1 detection based on other lectins [61–63]. Additionally, MUC1 aptamer and MUC1 antibody can be used to provide higher analytical performances as found in the literature [64–67]. But especially using aptamers or antibodies will enhance the cost of production.

There are conventional immunoanalytical techniques and kits for accurate determination of MUC1. However, these are commonly based on enzyme linked immunosorbent assay (ELISA) methods that need expensive immune-chemicals, long response times and experienced people [68–70]. In this manner, molecular imprinted polymer technology can be a good alternative for the development of electrochemical affinity sensors for detection of biomarkers with high selectivity [71]. This technique is a new trend for creating “biomimetic receptors”. When molecular imprinted polymers were synthesizing, a template molecule was used to form artificial cavities specifically. Therefore, MIP-based systems have not only provided shape or dimensional biomimetic platform, but also provides complementary electrostatic environment [72–74].

Molecular imprinted polymers can be a good alternative in order to develop polymer based synthetic receptors for label free detection of biomolecules. For example, Ramanaviciene et al. worked on a molecular imprinted polymer based label-free detection system that is for bovine leukemia virus glycoprotein recognition and they received very effective results in compared with spectrophotometrical data [75], Zhao et al. developed molecular imprinted polymer beads for label free detection of bovine hemoglobin with high selectivity and specificity [76], Wang et al. reported boronate affinity based molecular imprinted polymers for antibody and label free detection of glycoproteins multiplexly [77].

Conductive polymers can be chosen for enhancing analytical characteristics of a biosensor with the aid of their electrochemical activity, conductivity, stability and biocompatibility properties. The most commonly used conductive polymers are polyaniline, polypyrrole, polythiophene and poly(3,4-ethylenedioxythiophene) in the design of biosensors [78,79]. For example, in order to detect some biomolecules, Ramanaviciene et al. [75], Ramanavicius et al. used poly-pyrrole for electrochemical biosensor design [80]. Dutta et al. worked on

polyaniline-based biosensors [81], Chu et al. designed molecular imprinted polyaniline nanowire-based biosensors [82].

All these probabilities of developments were connected with funding opportunities and laboratory equipments. However, there are still many research ideas on these valuable topics to create the best and fastest detection method for cancers.

**Supplementary Materials:** The following are available online at <https://www.mdpi.com/article/10.3390/nanomanufacturing1010003/s1>, Figure S1: SEM images of p(HEMA)-IMEO-ConA nanoparticles (10 kx, 50 kx, 100 kx); Figure S2: AFM images of (A) p(HEMA) and (B) p(HEMA)-IMEO nanoparticles; Figure S3: FTIR spectrum analysis of p(HEMA), p(HEMA)-IMEO and p(HEMA)-IMEO-ConA; Figure S4: Zeta size results of (A) p(HEMA) and (B) p(HEMA)-IMEO-ConA nanoparticles; Figure S5: Zeta potential results of (A) p(HEMA) and (B) p(HEMA)-IMEO-ConA nanoparticles; Figure S6: CV analysis of p(HEMA)-IMEO-ConA with different MUC1 concentrations (5  $\mu$ L p(HEMA)-IMEO-ConA nanopolymer, 25  $^{\circ}$ C, 90 min, different concentration of MUC1, 25  $^{\circ}$ C, 20 min); Figure S7: Storage stability results (5  $\mu$ L p(HEMA)-IMEO-ConA nanopolymer, 25  $^{\circ}$ C, 90 min, 10 U/mL MUC1, 25  $^{\circ}$ C, 20 min); Figure S8: Reproducibility results (5  $\mu$ L p(HEMA)-IMEO-ConA nanopolymer, 25  $^{\circ}$ C, 90 min, 10 U/mL MUC1 + 1 mM MnCl<sub>2</sub>, 1 mM CaCl<sub>2</sub> ion mixture, 25  $^{\circ}$ C, 20 min); Figure S9: Grubb test results from Graphpad Online tool; Figure S10: (A) Calibration curve of ELISA kit (0.25–8 ng/mL), (B) Comparison the results of nanobiosensor and MUC1 ELISA kit.

**Author Contributions:** F.U.-K. investigation, conceptualization, methodology, validation, writing, editing; S.A. supervising, writing, editing. All authors have read and agreed to the published version of the manuscript.

**Funding:** This work was supported by Ege University Scientific Research Project Coordination with project number 17 FBE 002. The authors are thankful to The Scientific and Technological Research Council of Turkey (TUBITAK) for 2211-C PhD Bursary Programme in Priority Areas for their supports to Fulden ULUCAN's PhD thesis.

**Institutional Review Board Statement:** Not applicable.

**Informed Consent Statement:** Not applicable.

**Data Availability Statement:** Data is contained within the article or Supplementary Material.

**Acknowledgments:** The authors would like to thank Cansu İlke KURU for her helpful advice and experiences during the research and experimental parts for this manuscript.

**Conflicts of Interest:** The authors declare no conflict of interest.

## References

1. Seyfried, T.N.; Shelton, L.M. Cancer as a metabolic disease. *Nutr. Metab.* **2010**, *7*. [CrossRef] [PubMed]
2. Siegel, R.L.; Miller, K.D.; Jemal, A. Cancer statistics, 2020. *CA Cancer J. Clin.* **2020**, *70*, 7–30. [CrossRef] [PubMed]
3. Siegel, R.L.; Miller, K.D.; Fuchs, H.E.; Jemal, A. Cancer Statistics, 2021. *CA Cancer J. Clin.* **2021**, *71*, 7–33. [CrossRef] [PubMed]
4. Cancer Statistics. Available online: <https://www.cancer.gov/about-cancer/understanding/statistics> (accessed on 13 April 2021).
5. Wang, L.V. Ultrasound-mediated biophotonic imaging: A review of acousto-optical tomography and photo-acoustic tomography. *Dis. Markers* **2003**, *19*, 123–138. [CrossRef]
6. Nam, E.J.; Yun, M.J.; Oh, Y.T.; Kim, J.W.; Kim, J.H.; Kim, S.; Jung, Y.W.; Kim, S.W.; Kim, Y.T. Diagnosis and staging of primary ovarian cancer: Correlation between PET/CT, Doppler US, and CT or MRI. *Gynecol. Oncol.* **2010**, *116*, 389–394. [CrossRef]
7. Guimaraes, M.D.; Schuch, A.; Hochegger, B.; Gross, J.L.; Chojniak, R.; Marchiori, E. Ressonância magnética funcional na oncologia: Estado da arte. *Radiol. Bras.* **2014**, *47*, 101–111. [CrossRef] [PubMed]
8. Tsukamoto, E.; Ochi, S. PET/CT today: System and its impact on cancer diagnosis. *Ann. Nucl. Med.* **2006**, *20*, 255–267. [CrossRef] [PubMed]
9. Schillaci, O.; Scimeca, M.; Toschi, N.; Bonfiglio, R.; Urbano, N.; Bonanno, E. Combining diagnostic imaging and pathology for improving diagnosis and prognosis of cancer. *Contrast Media Mol. Imaging* **2019**, *2019*. [CrossRef]
10. Tothill, I.E. Biosensors for cancer markers diagnosis. *Semin. Cell Dev. Biol.* **2009**, *20*, 55–62. [CrossRef] [PubMed]
11. Bădilă, E.; Japie, C.; Bartoș, D. Cancer biomarkers in clinical practice. *Rom. J. Intern. Med.* **2014**, *52*, 223–232. [PubMed]
12. Kirwan, A.; Utratna, M.; O'Dwyer, M.E.; Joshi, L.; Kilcoyne, M. Glycosylation-Based serum biomarkers for cancer diagnostics and prognostics. *BioMed Res. Int.* **2015**, *2015*. [CrossRef] [PubMed]
13. Singh, P.K.; Hollingsworth, M.A. Cell surface-associated mucins in signal transduction. *Trends Cell Biol.* **2006**, *16*, 467–476. [CrossRef] [PubMed]

14. Azhar Aziz, M. Mucin family genes are downregulated in colorectal cancer patients. *J. Carcinog. Mutagen.* **2014**, *S10*. [[CrossRef](#)]
15. Nath, S.; Mukherjee, P. MUC1: A multifaceted oncoprotein with a key role in cancer progression. *Trends Mol. Med.* **2014**, *20*, 332–342. [[CrossRef](#)] [[PubMed](#)]
16. Rachagani, S.; Torres, M.P.; Moniaux, N.; Batra, S.K. Current status of mucins in the diagnosis and therapy of cancer. *BioFactors* **2009**, *35*, 509–527. [[CrossRef](#)] [[PubMed](#)]
17. Jing, X.; Liang, H.; Hao, C.; Yang, X.; Cui, X. Overexpression of MUC1 predicts poor prognosis in patients with breast cancer. *Oncol. Rep.* **2019**, *41*, 801–810. [[CrossRef](#)] [[PubMed](#)]
18. Hossain, M.; Wall, K. Immunological evaluation of recent MUC1 glycopeptide cancer vaccines. *Vaccines* **2016**, *4*, 25. [[CrossRef](#)]
19. Nabavinia, M.S.; Gholoobi, A.; Charbgoos, F.; Nabavinia, M.; Ramezani, M.; Abnous, K. Anti-MUC1 aptamer: A potential opportunity for cancer treatment. *Med. Res. Rev.* **2017**, *37*, 1518–1539. [[CrossRef](#)]
20. Moreno, M.; Bontkes, H.J.; Scheper, R.J.; Kenemans, P.; Verheijen, R.H.M.; von Mensdorff-Pouilly, S. High level of MUC1 in serum of ovarian and breast cancer patients inhibits huHMFG-1 dependent cell-mediated cytotoxicity (ADCC). *Cancer Lett.* **2007**, *257*, 47–55. [[CrossRef](#)]
21. Rughetti, A.; Fama, A.; von Mensdorff-Pouilly, S.; Taurino, F.; Rahimi, H.; Ribersani, M.; Natalino, F.; D’Elia, G.M.; Bizzoni, L.; Latagliata, R.; et al. Circulating MUC1 levels (CA15.3) in Myeloproliferative Disorders (MPD). *Blood* **2008**, *112*, 5237. [[CrossRef](#)]
22. Gheybi, E.; Amani, J.; Salmanian, A.H.; Mashayekhi, F.; Khodi, S. Designing a recombinant chimeric construct contain MUC1 and HER2 extracellular domain for pre-diagnostic breast cancer. *Tumor Biol.* **2014**, *35*, 11489–11497. [[CrossRef](#)] [[PubMed](#)]
23. Florea, A.; Cristea, C.; Săndulescu, R. MUC1 marker for the detection of ovarian cancer. A review. *Farmacia* **2014**, *62*, 1–13.
24. Yousefi, M.; Dehghani, S.; Nosrati, R.; Zare, H.; Evazalipour, M.; Mosafer, J.; Tehrani, B.S.; Pasdar, A.; Mokhtarzadeh, A.; Ramezani, M. Aptasensors as a new sensing technology developed for the detection of MUC1 mucin: A review. *Biosens. Bioelectron.* **2019**, *130*, 1–19. [[CrossRef](#)] [[PubMed](#)]
25. Gökay, Ö.; Karakoç, V.; Andaç, M.; Türkmen, D.; Denizli, A. Dye-attached magnetic poly(hydroxyethyl methacrylate) nanospheres for albumin depletion from human plasma. *Artif. Cells Nanomed. Biotechnol.* **2015**, *43*, 62–70. [[CrossRef](#)] [[PubMed](#)]
26. Altay, C.; Senay, R.H.; Eksin, E.; Congur, G.; Erdem, A.; Akgol, S. Development of amino functionalized carbon coated magnetic nanoparticles and their application to electrochemical detection of hybridization of nucleic acids. *Talanta* **2017**, *164*, 175–182. [[CrossRef](#)] [[PubMed](#)]
27. Bangs, L.B. *Uniform Latex Particles*; Seragen Diagnostic Inc.: Indianapolis, IN, USA, 1984.
28. Elgrishi, N.; Rountree, K.J.; McCarthy, B.D.; Rountree, E.S.; Eisenhart, T.T.; Dempsey, J.L. A Practical Beginner’s Guide to Cyclic Voltammetry. *J. Chem. Educ.* **2018**, *95*, 197–206. [[CrossRef](#)]
29. Becker, J.W.; Edelman, G.M.; Reeke, N.; Wang, J.L.; Cunningham, B.A. The covalent concanavalin structure of the monomer. *Biol. Chem.* **1975**, *260*, 1513–1524. [[CrossRef](#)]
30. Kaushik, S.; Mohanty, D.; Surolia, A. The role of metal ions in substrate recognition and stability of concanavalin A: A molecular dynamics study. *Biophys. J.* **2009**, *96*, 21–34. [[CrossRef](#)]
31. Kumari, K.; Yadav, S. Linear regression analysis study. *J. Pract. Cardiovasc. Sci.* **2018**, *4*, 33. [[CrossRef](#)]
32. Shrivastava, A.; Gupta, V. Methods for the determination of limit of detection and limit of quantitation of the analytical methods. *Chron. Young Sci.* **2011**, *2*, 21. [[CrossRef](#)]
33. Rodríguez, L.C.; Campa[nbreve]Ta, A.M.G.; Linares, C.J.; Ceba, M.R. Estimation of performance characteristics of an analytical method using the data set of the calibration experiment. *Anal. Lett.* **1993**, *26*, 1243–1258. [[CrossRef](#)]
34. Rao, T.N. Validation of analytical methods. In *Calibration and Validation of Analytical Methods—A Sampling of Current Approaches*; InTechOpen: London, UK, 2018. [[CrossRef](#)]
35. Aslam, M. Introducing Grubbs’s test for detecting outliers under neutrosophic statistics—An application to medical data. *J. King Saud Univ. Sci.* **2020**, *32*, 2696–2700. [[CrossRef](#)]
36. European Medicines Agency. ICH validation of analytical methods: Methodology. *ICH Q2B* **1996**, *53*, 128–143.
37. Pandey, R. Commonly used *t*-tests in medical research. *J. Pract. Cardiovasc. Sci.* **2015**, *1*, 185. [[CrossRef](#)]
38. Hazra, A. Using the confidence interval confidently. *J. Thorac. Dis.* **2017**, *9*, 4125–4130. [[CrossRef](#)] [[PubMed](#)]
39. AN Analytical Methods Committee. Using the grubbs and cochrane tests to identify outliers. *Anal. Methods* **2015**, *7*, 7948–7950. [[CrossRef](#)]
40. Yılmaz, A. *Turklab—Kalibrasyon ve Deney Laboratuvarları Derneği Turklab Rehber 01 Kimyasal Analizlerde Metot Validasyonu ve Verifikasyonu*; Turklab: Menderes, Turkey, 2013; pp. 1–51. Available online: [http://turklab.org/tr/TURKLAB\\_Rehber\\_01\\_Rev.2.pdf](http://turklab.org/tr/TURKLAB_Rehber_01_Rev.2.pdf) (accessed on 13 April 2021).
41. Bhushan, B.C. Surface roughness analysis and measurement techniques. *Mod. Tribol. Handb. Vol. One Princ. Tribol.* **2000**, 49–119. [[CrossRef](#)]
42. Rajesh Kumar, B.; Subba Rao, T. AFM studies on surface morphology, topography and texture of nanostructured zinc aluminum oxide thin films. *Dig. J. Nanomater. Biostruct.* **2012**, *7*, 1881–1889.
43. De, R.R.L.; Albuquerque, D.A.C.; Cruz, T.G.S.; Yamaji, F.M.; Leite, F.L. Measurement of the Nanoscale Roughness by Atomic Force Microscopy: Basic Principles and Applications. *At. Force Microsc. Imaging Meas. Manip. Surfaces At. Scale* **2012**. [[CrossRef](#)]
44. Webb, H.K.; Truong, V.K.; Hasan, J.; Fluke, C.; Crawford, R.J.; Ivanova, E.P. Roughness parameters for standard description of surface nanoarchitecture. *Scanning* **2012**, *34*, 257–263. [[CrossRef](#)] [[PubMed](#)]

45. Toprak, A.; Görgün, C.; Kuru, C.I.; Türkcan, C.; Uygun, M.; Akgöl, S. Boronate affinity nanoparticles for RNA isolation. *Mater. Sci. Eng. C* **2015**, *50*, 251–256. [[CrossRef](#)] [[PubMed](#)]
46. Demir, E.F.; Kuru, C.I.; Uygun, M.; Aktaş Uygun, D.; Akgöl, S. Antibody separation using lectin modified poly(HEMA-EDMA) hydrogel membranes. *J. Biomater. Sci. Polym. Ed.* **2018**, *29*, 344–359. [[CrossRef](#)] [[PubMed](#)]
47. Karmakar, S. Particle size distribution and zeta potential based on dynamic light scattering: Techniques to characterize stability and surface charge distribution of charged colloids. *Recent Trends Mater. Phys. Chem.* **2019**, 117–139.
48. Wang, P.; Keller, A.A. Natural and engineered nano and colloidal transport: Role of zeta potential in prediction of particle deposition. *Langmuir* **2009**, *25*, 6856–6862. [[CrossRef](#)]
49. Suttiponparnit, K.; Jiang, J.; Sahu, M.; Suvachittanont, S.; Charinpanitkul, T.; Biswas, P. Role of surface area, primary particle size, and crystal phase on titanium dioxide nanoparticle dispersion properties. *Nanoscale Res. Lett.* **2011**, *6*, 1–8. [[CrossRef](#)] [[PubMed](#)]
50. Njobuenwu, D. Determination of contact angle from contact area of liquid droplet spreading on solid substrate. *Leonardo Electron. J. Pract. Technol.* **2007**, *6*, 29–38.
51. Nawaz, M.A.H.; Rauf, S.; Catanante, G.; Nawaz, M.H.; Nunes, G.; Marty, J.L.; Hayat, A. One step assembly of thin films of carbon nanotubes on screen printed interface for electrochemical aptasensing of breast cancer biomarker. *Sensors* **2016**, *16*, 1651. [[CrossRef](#)] [[PubMed](#)]
52. Altintas, Z.; Kallempudi, S.S.; Sezerman, U.; Gurbuz, Y. A novel magnetic particle-modified electrochemical sensor for immunosensor applications. *Sens. Actuators B Chem.* **2012**, *174*, 187–194. [[CrossRef](#)]
53. Li, H.; He, J.; Li, S.; Turner, A.P.F. Electrochemical immunosensor with N-doped graphene-modified electrode for label-free detection of the breast cancer biomarker CA 15-3. *Biosens. Bioelectron.* **2013**, *43*, 25–29. [[CrossRef](#)] [[PubMed](#)]
54. Ding, Y.; Ling, J.; Wang, H.; Zou, J.; Wang, K.; Xiao, X.; Yang, M. Fluorescent detection of Mucin 1 protein based on aptamer functionalized biocompatible carbon dots and graphene oxide. *Anal. Methods* **2015**, *7*, 7792–7798. [[CrossRef](#)]
55. Zhang, J.; Ran, F.; Zhou, W.; Shang, B.; Yu, F.; Wu, L.; Hu, W.; He, X.; Chen, Q. Ultrasensitive fluorescent aptasensor for MUC1 detection based on deoxyribonuclease I-aided target recycling signal amplification. *RSC Adv.* **2018**, *8*, 32009–32015. [[CrossRef](#)]
56. Hong, C.; Yuan, R.; Chai, Y.; Zhuo, Y. Ferrocenyl-doped silica nanoparticles as an immobilized affinity support for electrochemical immunoassay of cancer antigen 15-3. *Anal. Chim. Acta* **2009**, *633*, 244–249. [[CrossRef](#)] [[PubMed](#)]
57. Sumbuloglu, K.; Sumbuloglu, V. *Biyoistatistik*; Hatipoglu Press: Ankara, Turkey, 2007.
58. Liu, B.; Cang, H.; Jin, J. Molecularly imprinted polymers based electrochemical sensor for 2,4-dichlorophenol determination. *Polymers* **2016**, *8*, 309. [[CrossRef](#)] [[PubMed](#)]
59. Kiss, L.; David, V.; David, I.G.; Lazăr, P.; Mihailciuc, C.; Stamatina, I.; Ciobanu, A.; Ștefănescu, C.D.; Nagy, L.; Nagy, G.; et al. Electropolymerized molecular imprinting on glassy carbon electrode for voltammetric detection of dopamine in biological samples. *Talanta* **2016**, *160*, 489–498. [[CrossRef](#)] [[PubMed](#)]
60. Rauf, S.; Mishra, G.K.; Azhar, J.; Mishra, R.K.; Goud, K.Y.; Nawaz, M.A.H.; Marty, J.L.; Hayat, A. Carboxylic group riched graphene oxide based disposable electrochemical immunosensor for cancer biomarker detection. *Anal. Biochem.* **2018**, *545*, 13–19. [[CrossRef](#)] [[PubMed](#)]
61. Terävä, J.; Tiainen, L.; Lamminmäki, U.; Kellokumpu-Lehtinen, P.-L.; Pettersson, K.; Gidwani, K. Lectin nanoparticle assays for detecting breast cancer-associated glycovariants of cancer antigen 15-3 (CA15-3) in human plasma. *PLoS ONE* **2019**, *14*, e0219480. [[CrossRef](#)]
62. Choi, J.W.; Moon, B.I.; Lee, J.W.; Kim, H.J.; Jin, Y.; Kim, H.J. Use of CA15-3 for screening breast cancer: An antibody-lectin sandwich assay for detecting glycosylation of CA15-3 in sera. *Oncol. Rep.* **2018**, *40*, 145–154. [[CrossRef](#)] [[PubMed](#)]
63. Park, Y.M.; Kim, S.J.; Kim, K.; Han, Y.D.; Yang, S.S.; Yoon, H.C. Lectin-based optical sensing for quantitative analysis of cancer antigen CA15-3 as a breast cancer marker. *Sens. Actuators B Chem.* **2013**, *186*, 571–579. [[CrossRef](#)]
64. Karpik, A.E.; Crulhas, B.P.; Rodrigues, C.B.; Castro, G.R.; Pedrosa, V.A. Aptamer-based biosensor developed to monitor MUC1 released by prostate cancer cells. *Electroanalysis* **2017**, *29*, 2246–2253. [[CrossRef](#)]
65. Shekari, Z.; Zare, H.R.; Falahati, A. Dual assaying of breast cancer biomarkers by using a sandwich-type electrochemical aptasensor based on a gold nanoparticles–3D graphene hydrogel nanocomposite and redox probes labeled aptamers. *Sens. Actuators B Chem.* **2021**, *332*, 129515. [[CrossRef](#)]
66. Akbari Nakhjavani, S.; Khalilzadeh, B.; Samadi Pakchin, P.; Saber, R.; Ghahremani, M.H.; Omid, Y. A highly sensitive and reliable detection of CA15-3 in patient plasma with electrochemical biosensor labeled with magnetic beads. *Biosens. Bioelectron.* **2018**, *122*, 8–15. [[CrossRef](#)] [[PubMed](#)]
67. Selwyn, P.G.C.; Loganathan, P.R.; Begam, K.H. Development of electrochemical biosensor for breast cancer detection using gold nanoparticle doped CA 15-3 antibody and antigen interaction. In Proceedings of the 2013 International Conference on Signal Processing, Image Processing & Pattern Recognition, Coimbatore, India, 7–8 February 2013; pp. 75–81.
68. Ferreira, C.S.M.; Papamichael, K.; Guilbault, G.; Schwarzacher, T.; Garipey, J.; Missailidis, S. DNA aptamers against the MUC1 tumour marker: Design of aptamer–antibody sandwich ELISA for the early diagnosis of epithelial tumours. *Anal. Bioanal. Chem.* **2008**, *390*, 1039–1050. [[CrossRef](#)]
69. Falahat, R.; Wiranowska, M.; Gallant, N.D.; Toomey, R.; Hill, R.; Alcantar, N. A Cell ELISA for the quantification of MUC1 mucin (CD227) expressed by cancer cells of epithelial and neuroectodermal origin. *Cell. Immunol.* **2015**, *298*, 96–103. [[CrossRef](#)] [[PubMed](#)]
70. Song, J.; Zhou, Y.; Chen, B.; Lou, W.; Gu, J. Development of electrochemical aptamer biosensor for tumor marker MUC1 determination. *Int. J. Electrochem. Sci.* **2017**, *12*, 5618–5627. [[CrossRef](#)]

71. Crapnell, R.D.; Dempsey-Hibbert, N.C.; Peeters, M.; Tridente, A.; Banks, C.E. Molecularly imprinted polymer based electrochemical biosensors: Overcoming the challenges of detecting vital biomarkers and speeding up diagnosis. *Talanta Open* **2020**, *2*, 100018. [[CrossRef](#)]
72. Farré, M.; Barceló, D. Sensor, biosensors and MIP based sensors. In *Food Toxicants Analysis Techniques, Strategies and Developments*; Pico, Y., Ed.; Elsevier: Amsterdam, The Netherlands, 2007; pp. 599–636. [[CrossRef](#)]
73. Ramanavicius, S.; Jagminas, A.; Ramanavicius, A. Advances in molecularly imprinted polymers based affinity sensors (review). *Polymers* **2021**, *13*, 974. [[CrossRef](#)] [[PubMed](#)]
74. Uygun, Z.O.; Ertugrul Uygun, H.D.; Ermis, N.; Canbay, E. Molecularly imprinted sensors—New sensing technologies. *Biosens. Micro Nanoscale Appl.* **2015**, 85–108. [[CrossRef](#)]
75. Ramanaviciene, A.; Ramanavicius, A. Molecularly imprinted polypyrrole-based synthetic receptor for direct detection of bovine leukemia virus glycoproteins. *Biosens. Bioelectron.* **2004**, *20*, 1076–1082. [[CrossRef](#)]
76. Zhao, Y.-J.; Zhao, X.-W.; Hu, J.; Li, J.; Xu, W.-Y.; Gu, Z.-Z. Multiplex Label-Free Detection of Biomolecules with an Imprinted Suspension Array. *Angew. Chemie Int. Ed.* **2009**, *48*, 7350–7352. [[CrossRef](#)]
77. Wang, H.; Xu, Q.; Shang, L.; Wang, J.; Rong, F.; Gu, Z.; Zhao, Y. Boronate affinity molecularly imprinted inverse opal particles for multiple label-free bioassays. *Chem. Commun.* **2016**, *52*, 3296–3299. [[CrossRef](#)] [[PubMed](#)]
78. Ramanavicius, S.; Ramanavicius, A. Conducting Polymers in the Design of Biosensors and Biofuel Cells. *Polymers* **2020**, *13*, 49. [[CrossRef](#)] [[PubMed](#)]
79. Aydemir, N.; Malmström, J.; Trivas-Sejdic, J. Conducting polymer based electrochemical biosensors. *Phys. Chem. Chem. Phys.* **2016**, *18*, 8264–8277. [[CrossRef](#)] [[PubMed](#)]
80. Ramanavicius, A.; Oztekin, Y.; Ramanaviciene, A. Electrochemical formation of polypyrrole-based layer for immunosensor design. *Sens. Actuators B Chem.* **2014**, *197*, 237–243. [[CrossRef](#)]
81. Dutta, R.; Thangapandi, K.; Mondal, S.; Nanda, A.; Bose, S.; Sanyal, S.; Jana, S.K.; Ghorai, S. Polyaniline based electrochemical sensor for the detection of dengue virus infection. *Avicenna J. Med. Biotechnol.* **2020**, *12*, 77–84. [[PubMed](#)]
82. Chu, T.-X.; Vu, V.-P.; Tran, H.-T.; Tran, T.-L.; Tran, Q.-T.; Le Manh, T. Molecularly imprinted polyaniline nanowire-based electrochemical biosensor for chloramphenicol detection: A kinetic study of aniline electropolymerization. *J. Electrochem. Soc.* **2020**, *167*, 027527. [[CrossRef](#)]